Chapter 14

A Miscellany of Applications

Applications are not totally absent from the preceding chapters; they appear now and then either to provide some relief from the mathematical development or to illustrate particular points. Some of them, and the sections where they are discussed, are listed below.

Red sunsets and blue moons (4.4).
Polarization of skylight (5.7).
Rainbow (7.2, 13.1).
Haloes (7.3).
Scattering by fibers (8.4).
Christiansen effect (11.2).
Sphere in a waveguide (11.4).
Levitation by radiation pressure (11.4).
Asymmetry of interstellar absorption bands (11.5).
Colors of colloidal gold (12.4).
Electron–hole droplets in germanium (12.4).
Particle sizing (13.5).
Biological particles (13.8).
Ocean waters (13.8).

This chapter merely contains a greater concentration of applications.

A separate volume could be devoted solely to applications. Indeed, it would be a volume almost without end because the rate at which we can evaluate and write about them is less than the rate at which new ones are being devised or old ones are being refined. This chapter is of necessity limited in scope. We have been selective, concentrating our efforts on those topics most familiar or of greatest interest to us. No attempt has been made to be comprehensive or to achieve a balanced treatment. We have, however, favored topics that illustrate points stressed particularly heavily in preceding chapters.

We begin with a discussion of optical constants, which are needed in almost all applications. A treatment of atmospheric aerosols is followed by two other topics from atmospheric science: inferences about noctilucent clouds—clouds at the edge of space—made on the basis of polarization measurements; and measuring rainfall with radar. A discussion of interstellar dust—particles in the "cosmic laboratory"—is followed by an earthbound laboratory investigation in which the advantages of small particles are exploited in high-pressure studies of optical spectra. The final topics have a biological flavor: the Giaever immunological slide, an application of surface modes in small metallic particles; and the effects of microwave radiation on macromolecules.

14.1 THE PROBLEM OF OPTICAL CONSTANTS

We have emphasized that the wavelength-dependent optical constants are the fundamental quantities that determine the macroscopic optical properties of matter. Because of this, optical constants are required in many applications of absorption and scattering of light by small particles: they are needed for determining optical properties of smog particles and mineral grains in the atmosphere, dust grains in interstellar space, phytoplankton in the ocean, and biological cells. It is little wonder then that scientists in many disciplines spend so much time searching through the physics, chemistry, and mineralogy journals (to name a few sources) for the optical constants they need.

14.1.1 Homogeneous Sample

Determination of optical constants is not necessarily an easy task, even for homogeneous solids and liquids at room temperature, particularly in spectral regions of very high or very low absorption. Optical constants are not directly measurable but must be inferred, sometimes rather circuitously, by analyzing primary measurements (e.g., transmission and reflection) with theoretical expressions (e.g., the Fresnel formulas). A brief survey of methods for determining optical constants of bulk matter has been given in Section 2.9. These techniques require homogeneous samples of a size and shape such that the conditions underlying the validity of the theory used for analyzing measurements are satisfied; examples are large, single crystals, slabs of glassy or amorphous solids, and liquid-filled cuvettes. Unfortunately, many solids are commonly obtainable only as small particles (i.e., powders). It is much more difficult to determine optical constants for these materials even if the powder sample contains only a single component. Lack of accurate optical constants for powdered materials arises not so much from want of effort as from the complexity of data analysis.

14.1.2 Powder Samples

To determine optical constants of powder samples requires one or more measurements of transmission, or diffuse reflection, or scattering, and an

appropriate theoretical model, such as a theory of diffuse reflection or Mie theory. In principle these measurements are not difficult to make. But the appropriateness of the theoretical models used to analyze these measurements is sometimes doubtful. For example, if one desired infrared ($\sim$ 10 μm) optical constants of quartz, one could measure transmission by a dilute suspension of fine quartz powder in a transparent KBr matrix and reflection from a pressed sample (e.g., Volz, 1972). Analysis of the transmission measurements might be based on Mie theory or one of its approximations, and the reflectance data might be analyzed with the Fresnel formulas. Neither of these two theories, however, is applicable. Quartz particles are highly irregular and their extinction spectrum is quite different from that of spheres (see Fig. 12.14). And the Fresnel formulas are not applicable because the quartz powder cannot be compressed into a homogeneous solid with a smooth surface. Even with accurate measurements, therefore, these two theories would quite likely yield highly erroneous optical constants. Pressed samples of softer materials, such as potassium bromide, may, however, approach single-crystal density and have rather smooth surfaces. For such materials these methods have been used with some success (Tomaselli et al., 1981). But for harder materials (and anisotropic solids) serious problems remain.

Optical constants can be inferred from analysis of measurements on single spheres or highly monodisperse collections of spheres. For example, angular scattering by colloidal suspensions of polystyrene spheres has been used frequently to determine both their size and refractive index at wavelengths where polystyrene is weakly absorbing. Measurements on single, homogeneous, perfectly spherical particles can be analyzed with Mie theory as confidently as measurements of reflectances at smooth plane interfaces can be analyzed with the Fresnel formulas. Pluchino et al. (1980), for example, determined the complex refractive index of carbon at a single wavelength in the visible by levitating a carbon sphere a few micrometers in diameter, measuring the angular light scattering, and fitting their data with Mie theory. A similar technique has been used by Wyatt (1980), although for inhomogeneous particles. As techniques for levitating single particles and measuring scattering patterns come into wider use, obtaining optical constants from measurements on single particles will surely become more common. In general, however, this is practically limited to particles of simple shape such as spheres or long, circular cylinders.

14.1.3 Optical Constants from Absorption Measurements

An approach widely used by atmospheric scientists is to infer the imaginary part of the refractive index k from measurements of the absorption coefficient α of particulate samples. Diffuse reflection, the photoacoustic effect, and integrating plates have been used for determining absorption even in the presence of considerable scattering; these methods are discussed briefly in the following section. The relation (2.52) between α and k, $\alpha = 4\pi k/\lambda$, is, of course, strictly valid only for homogeneous media. But under some circum-

stances its use for inhomogeneous media is justified. For example, it follows from (3.47), (3.48), and (12.9) that transmission by a dilute suspension of spheres small compared with the wavelength is approximately

$$\frac{I}{I_0} = \exp\left[-\frac{4\pi k}{\lambda}\frac{9n}{(n^2+2)^2}d\right] \tag{14.1}$$

provided that extinction is dominated by absorption, k is small, and n is not too large; $d = fh$, where f is the volume fraction of particles and h is the sample thickness. The expression containing n is about 1 at visible wavelengths for many common substances. For example, it is about 0.75 for $n = 1.5$, and can be made even closer to 1 by suitably choosing the medium in which the particles are suspended: n is the *relative* refractive index. Measurement of transmission and calculation of k from (14.1) is therefore approximately correct for dilute suspensions of Rayleigh spheres of many common materials with small k—hence the popularity of this procedure. But for several reasons, some of which have been discussed by Toon et al. (1976), (14.1) may be inapplicable:

1. Scattering may not be negligible, giving rise to apparent additional absorption.
2. The particles may not be small enough for the Rayleigh theory to be valid. For larger particles, the relation between absorption and size is more complicated.
3. The particles may not be spherical or, if spherical, they may agglomerate into nonspherical clumps. Contrary to much common opinion, absorption by Rayleigh particles can be quite shape dependent, as we have shown in Chapter 12.
4. The optical constants n and k are not independent: if k varies strongly, so must n. Either n must be measured by some other method or a theory of optical constants that couples them together properly must be used, such as the oscillator model (9.25) or the Kramers–Kronig relations [(2.49), (2.50)].

While inferring k from measurements of absorption by particulate samples may be valid for many kinds of solids at visible wavelengths, it may not be valid in spectral regions where the optical constants rapidly vary, such as the infrared or far ultraviolet.

14.1.4 Powders of Anisotropic Solids

More problems must be faced when trying to extract optical constants from measurements on particles of anisotropic solids. Random orientation of the particles averages somehow the two or three sets of optical constants. We

showed in Section 5.6 that in the Rayleigh approximation the average extinction cross section of a randomly oriented anisotropic sphere is just the equally weighted sum of three cross sections, one for an isotropic sphere with each set of optical constants. But this prescription has not been shown to be correct for larger particles (see Section 8.2). Even if it were correct in general, however, it is still not clear how to extract from measurements absorption associated with each of the principal axes of the crystal. For example, the infrared extinction spectrum of randomly oriented anisotropic particles such as calcite will show various bands. But without knowing which band is associated with which principal axis, it does not appear possible to extract the different sets of optical constants; this problem was recognized and discussed by Aronson and Emslie (1980). To ignore anisotropy and simply determine "average" optical constants as though the solid were isotropic is only sweeping the problem under the rug. These optical constants could not necessarily be used to analyze experiments other than those from which they were derived. For example, they could not be used to calculate the reflectance of an oriented, single crystal of the material. Even the use of average optical constants to calculate extinction by randomly oriented particles of the same kind would give errors if the size distribution were appreciably different from that of the sample from which the optical constants were derived.

14.1.5 Mixtures of Particles

Up to this point we have had in mind only single-component particulate samples. But multicomponent mixtures are common, and because of the difficulty of properly treating each component the tendency has been to infer "average" or "effective" optical constants from measurements on such mixtures. Yet this is fraught with difficulties. The measurements from which these optical constants are obtained, such as reflection or scattering or absorption, are not additive. Nor are optical constants additive. Hence, optical constants of mixtures determined by, for example, measuring absorption by particles in a matrix and reflection by a pressed surface cannot necessarily be used to predict correctly angular scattering by the particles. Despite these difficulties and the warnings issued by some, the deceptively simple procedure of determining a single set of optical constants for complex multicomponent mixtures of possibly anisotropic particles and then using such optical constants in all kinds of predictive calculations has been widespread. Optical constants of moon rocks consisting of many individual mineral components have often been used by astronomers in calculations relating to interplanetary or interstellar dust. Optical constants obtained for atmospheric dust have been used to predict possible climatic change; this is discussed further in the following section.

To conclude, we venture to state that the problem of how to determine accurate optical constants from measurements on particulate samples, in contrast with homogeneous solids and liquids, has not been solved in general, even for single-component powders. This does not mean that there have not

been successful determinations of optical constants for some particulate materials. It is simply that extracting optical constants from measurements on such materials is not generally possible in all spectral regions and for all kinds of samples, which may be multicomponent mixtures of nonspherical and anisotropic particles.

14.2 ATMOSPHERIC AEROSOLS

Atmospheric aerosols usually means the solid and liquid particles in the earth's atmosphere, excluding the solid and liquid water particles in clouds, fog, and rain. Although very tenuous and highly variable, they act as condensation nuclei for cloud droplets, alter the optical properties of clouds, and possibly play a role in the formation of smog and acid rain. And an understanding of their optical properties is needed for many applications:

Climate may be modified by both natural and human-made aerosols. Optical techniques are being used increasingly for remote sensing of the atmosphere as well as for communication. The military importance of aerosols has increased greatly because of surveillance, using both visible and infrared radiation, from satellites and because of missile guidance with light beams. This in turn has stimulated development of countermeasures—shielding against enemy surveillance and laser-guided missiles—and has renewed interest in an old trick—throwing out smoke screens.

From among all the possible applications of light scattering by atmospheric aerosols we have selected only a few. We begin with the intriguing question of what effect these particles may have on the earth's climate. Then we discuss some of what is known about their chemical composition and optical properties and how these are obtained by various methods: *in situ* measurements; collecting particles; and remotely sensing them. This is followed by a discussion of the problem of characterizing the complex mixture of particles that is the atmospheric aerosol. Finally, we briefly discuss the possibility of monitoring the global wind by measuring the Doppler shift of infrared radiation backscattered by atmospheric particles.

14.2.1 Effect of Aerosols on Climate

A controversy with possibly far-reaching consequences concerns the impact of atmospheric particles on the earth's climate. Temperature is one of the most easily monitored indicators of climatic change. Among the many discussions of the effects of aerosols on the global mean temperature, we direct the reader to the monograph by Twomey (1977) and the paper by Toon and Pollack (1980), from which some of the following is taken.

Typical changes in the global mean temperature over the past 1000 years seem to have been of order 1°C, although climate has changed considerably as in the "Little Ice Age" from about A.D. 1500 to 1900. The difference between average Ice Age (1.75 million to 10,000 years ago) temperatures and the

present-day average is thought to be about 5°C. More recently, during the late Stone Age, temperatures were perhaps 2.5°C higher than at present. Since human beings can adapt readily to temperature changes of tens of degrees such small excursions might at first glance appear inconsequential. Ocean levels, however, may have lowered about 100 m during the Ice Age because of storage of vast quantities of water in continental ice sheets. Coastal residents can surely appreciate that sea level changes of this magnitude could be catastrophic. Global mean temperature changes of even a few tenths of a degree may thus be of consequence. Particulate pollution is increasing, and it is therefore prudent to understand how such particles may affect the heat balance of our planet. Given the present state of knowledge, however, it is not certain if man's impact will be to increase or to decrease the global mean temperature.

The simplest view is that absorption by particles tends to heat the atmosphere while scattering into the backward hemisphere tends to cool it; thus, the two most important optical properties of aerosols as far as climatic change is concerned are absorption and backscattering. This simple view is complicated somewhat by the fact that aerosols exist primarily in two distinct atmospheric layers, the troposphere (from the ground up to about 10–20 km) and the stratosphere (between about 10–20 and 50 km). The troposphere is thermally coupled to the earth's surface rather strongly, whereas the stratosphere is not. Because of their thermal isolation, therefore, stratospheric particles tend to cool the earth's surface both by backscattering and absorbing solar radiation. Of less importance, but still appreciable, are thermal infrared effects of particles, particularly in the 8- to 12-μm "window" region, where the major atmospheric gases are highly transparent. It is in this wavelength region that the Planck function peaks for normal terrestrial temperatures. Upwelling infrared radiation from the earth's surface is therefore partly hindered from escaping into space because some particles have strong absorption bands in this spectral region. Thus, aerosols contribute to the so-called "greenhouse effect." Infrared radiation emitted toward the earth's surface by stratospheric particles may cause some warming in the lower atmosphere, thereby countering to some extent the cooling they cause by backscattering and absorbing solar radiation.

Various models have been proposed to predict the effect of atmospheric aerosols on the global mean temperature. The single-scattering albedo (i.e., the ratio of scattering to extinction) of such particles is a crucial parameter in these models because a high value will result in cooling, whereas a low value will result in warming; critical values—the boundary between high and low—from about 0.7 to 0.95 can be found in the literature. A value of 0.85 derived by Hansen et al. (1979) is being widely used. Charlock and Sellers (1980) arrived at a critical single-scattering albedo of 0.81.

Because the single-scattering albedo depends sensitively on the imaginary part of the refractive index there has been keen interest in determining optical constants of atmospheric particles. These are used to calculate the important parameters in the heat balance problem for present and predicted aerosol

loadings. A path commonly followed is to measure optical properties of atmospheric aerosols, either remotely (e.g., solar extinction and bistatic lidar scattering) or on collected samples (e.g., absorption and diffuse reflection), and infer optical constants from theoretical models. The optical constants so obtained are then used as input to Mie theory incorporated into heat balance calculations. But this path is strewn with many potential hazards, which may invalidate the final results. We shall discuss some of these hazards in following paragraphs. Directly measuring absorption and scattering by aerosols *in situ* is less fraught with pitfalls, but we delay our discussion of this until we have surveyed the chemical composition and absorptive properties of aerosol particles; this survey, taken from laboratory measurements on homogeneous samples, serves to give a feeling for expected values of k.

14.2.2 Absorption by Constituents of the Atmospheric Aerosol

Among the reasons it is difficult to predict the effect of particles on climate is that their composition and distribution are poorly known. The main types of known atmospheric particles are listed in Table 14.1.

The dominant aerosol in the lower atmosphere is windblown dust composed mostly of mineral particles together with some organic matter. Although they

Table 14.1 Constituents of the Atmospheric Aerosol

Constituent	Size	Comments
Windblown Surface Dust		
Quartz		
Calcite		
Oxides of iron	1–10 μm	~ 30% globally
Clay minerals		
Montmorillonite		
Illite		
Sea Spray		
Salt	1–10 μm	10–15% globally
Organic particles		
Sulfur Compounds		
Ammonium sulfate	~ 0.1 μm	Mostly stratospheric;
Sulfuric acid		50% globally
Volcanic Ash		Stratospheric; following volcanic activity
Others		
Anthropogenic and natural carbon		
Organic materials from vegetation		
Photochemical smog		

are fairly large, with consequently high settling rates, under some conditions these dust particles can spread far from their source and remain in the atmosphere for long periods. A notable example is dust from the Sahara, which spreads across much of the Atlantic Ocean between Africa and the Caribbean during summer months (Carlson and Benjamin, 1980). Dominating the marine aerosol are salt particles, together with some organic particles of marine origin; Blanchard (1967) has given a fascinating account of how these salt particles enter the atmosphere. The globally dominant mass of particles, found distributed over the entire earth, is composed of sulfur compounds, including ammonium sulfate and sulfuric acid. These particles are formed mostly in the stratosphere by complex chemical reactions. In periods of strong volcanic activity, volcanic ash may be appreciable, remaining in the atmosphere for several years after its introduction. Minor constituents of the atmospheric aerosol include terrestrial organic substances such as terpenes, and pollution such as carbon, metal oxides, and photochemical smog.

The many difficulties inherent in determining optical constants in regions of high absorption, especially for particulate samples, and the practical impossibility of obtaining accurate optical constants for complex mixtures of particles have been discussed in Section 14.1. These difficulties point to why it is worth considering measured optical constants of homogeneous materials that are known constituents of the atmospheric aerosol. Such measurements are not available for all constituents, in some instances because they are not obtainable in homogeneous bulk form. In Fig. 14.1 we show the imaginary part of the refractive index of several solids and liquids that are found as atmospheric particles. Results are given for water, ammonium sulfate, crystalline quartz, sulfuric acid, carbon, sodium chloride, and hematite (α-Fe_2O_3); to avoid clutter, only k values over limited spectral regions are given for most of these materials.

Except for carbon, there are two distinct spectral regions in which k is high (~ 1) for these materials: one in the infrared and the other in the ultraviolet, with a region of high transparency between. The reasons for this have been discussed in Section 10.4. To emphasize just how transparent these materials are in the intermediate region, we show with a dashed line the value of k for which a 1-cm-thick homogeneous sample would give 1% transmission, neglecting reflection losses at the boundaries. Only carbon, which has metal-like overlapping electronic energy bands (see Section 9.4), has consistently high k of order unity throughout the visible and infrared regions. The mineral hematite, although a very minor constituent of the atmospheric aerosol, is included because it is one of the very few highly absorbing (at visible wavelengths) substances known to be in the atmosphere.

The hatched region in Fig. 14.1 shows the approximate values of k at visible wavelengths inferred by various remote-sensing techniques (Grams et al., 1974; Reagan et al., 1980; and references cited therein). If we compare these values of k with those for individual constituents of the atmospheric aerosol, it seems

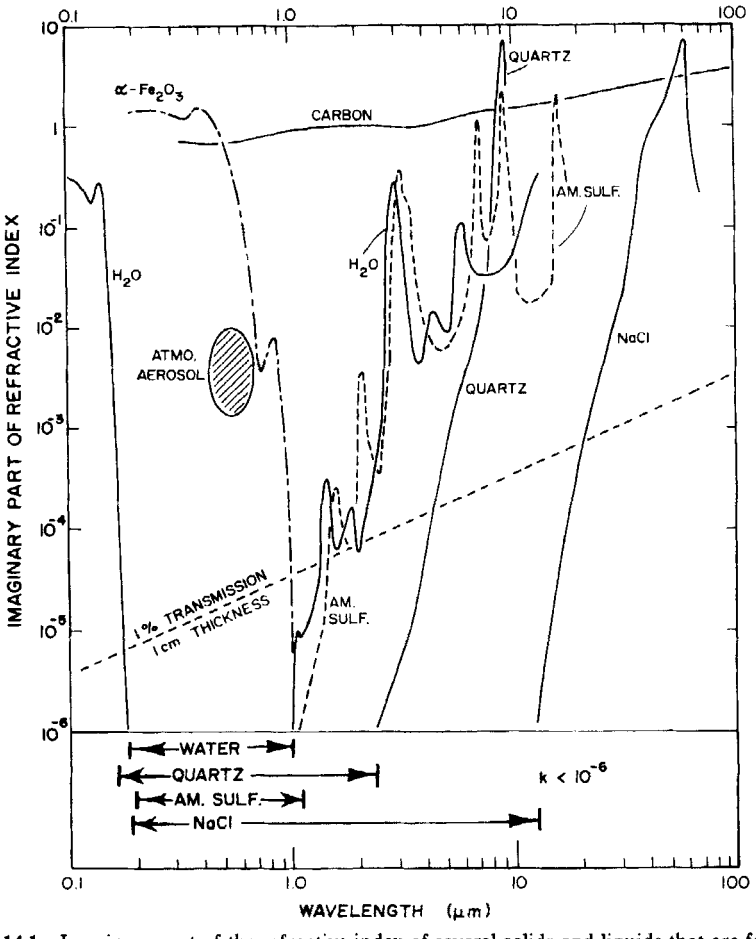

Figure 14.1 Imaginary part of the refractive index of several solids and liquids that are found as atmospheric particles.

clear that k determined remotely is some kind of average for a mixture containing a small amount of a strongly absorbing component such as carbon and much larger amounts of weakly absorbing components. Lindberg (1975) pointed this out after successfully matching measured spectral extinction by collected aerosol particles with calculations for mixtures of weakly absorbing minerals and about 0.5% carbon to give the required absorption. Thus the value $k = 0.001$ (for example) inferred from remote sensing should perhaps be looked upon as an average or effective k, but the averaging process and the subsequent uses to which this effective value is put must be examined critically. We shall return to this point later.

The possibility that carbon in small quantities is the dominant absorber in the atmospheric aerosol suggests looking for spectral features in carbon, which would provide a diagnostic test for this solid. Unfortunately, the absorption

spectrum of bulk carbon is rather featureless in the infrared and visible. The one spectral region where carbon, in small-particle form at least, has a prominent absorption feature is between 2200 and 2500 Å. Although this feature is not apparent in Fig. 14.1, absorption by small spheres of both graphite and glassy carbon rises to a pronounced peak where the real parts of their dielectric function are closest to -2. This feature in graphite particles, the surface plasmon absorption discussed at length in Section 12.1, is thought to be responsible for the dominant peak in the interstellar extinction spectrum (Fig. 14.4). Although it would be difficult to observe by remote sensing, a feature between 2200 and 2500 Å might be very useful in laboratory analysis for carbon particles in aerosol samples collected on filters, for example.

Because of the importance of the 8- to 12-μm atmospheric "window" region to the earth's heat balance, and in view of the many potential applications of CO_2 laser beams (9–11 μm) propagating in the atmosphere, we call attention to k in this region of the infrared. Note that several constituents of the atmospheric aerosol, including quartz and ammonium sulfate, have intense absorption bands associated with lattice vibrations. Other silicate minerals, including the clay minerals listed in Table 14.1, also have strong bands near 10 μm. These vibrational absorption bands are strong enough to give rise to the kind of highly shape-dependent absorption and scattering discussed in Chapter 12. Indeed, Fig. 12.14 displayed measurements on crystalline quartz dust to illustrate the extreme sensitivity of these bands to particle shape. The implications of these absorption bands in quartz and ammonium sulfate particles for remote sensing are discussed later.

14.2.3 In Situ Measurements of Absorption and Backscattering

Predicting optical properties of atmospheric aerosols from calculations for homogeneous, spherical particles leaves much to be desired. Mie theory may be a gross oversimplification. In addition, there may not be accurate optical constants for the constituents, even those that are known; and they may not all be known. Yet even minor constituents can be major contributors to absorption.

The most direct way of obtaining the two parameters most relevant to climatic change, absorption and backscattering, is to measure them for actual atmospheric aerosols. Backscattering can be derived from angular scattering measured *in situ* with a polar nephelometer (e.g., Grams, 1981) or with an integrating nephelometer. Measured extinction could, in principle, yield absorption. But if the aerosol particles are weakly absorbing, as is common, this requires taking the difference of two large quantities—scattering and extinction— of similar magnitude.

Absorption can be measured directly by the photoacoustic method. Although used most commonly for dense, highly absorbing aerosols (Bruce and Pinnick, 1977; Japar and Killinger, 1979; Roessler and Faxvog, 1979b), it has been proven to be feasible for measuring weak absorption of visible light by

ambient aerosols (Foot, 1979). A beam of direct sunlight was used as the source of modulated heating; and photoacoustic signals were measured alternately for ambient aerosols and for filtered air. This appears to be the only direct absorption measurement yet reported for atmospheric aerosols.

Direct measurement of absorption and backscattering at a sufficient number of sites to obtain a representative global average would be a step in the right direction toward assessing the impact of atmospheric particles on climate.

14.2.4 Sampling and Measurement

A less direct method of determining absorption by atmospheric particles is to collect them, on filters for example, and measure their absorption in the laboratory. In contrast with interstellar dust, atmospheric dust is sufficiently accessible to allow direct sampling and optical measurements. Yet the tenuousness of atmospheric aerosols leads to problems. Because of selective collecting lines and surfaces there may be differences between the sampled particles and those in the atmosphere. Evaporation of volatile compounds may occur, and contamination is always possible. And the state of aggregation will certainly change. Despite all this the advantages of a bird in the hand are substantial: time-consuming measurements can be done leisurely; particles can often be examined by electron or light microscopy to obtain their sizes and shapes; and chemical identification procedures can be used.

A major obstacle to determining absorption by collected particles is that scattering is often much greater than absorption. Some of the techniques devised to overcome this obstacle are shown schematically in Fig. 14.2; these are discussed very briefly in the following paragraphs.

Figure 14.2*a* shows the essential elements of a diffuse transmission technique (Fischer, 1970, 1973) that incorporates an integrating sphere—a sphere coated with a nonabsorbing, diffusely reflecting material (see Wendlandt and Hecht, 1966, Chap. 10). Measurements are made with and without the particulate sample (on a glass slide) in the light beam. From these measurements absorption can be obtained. A simpler arrangement (Lin et al., 1973) for accomplishing the same result, often called the integrating plate method, is shown in Fig. 14.2*b*. The particles are on an opal glass plate—a simple diffuser—which directs the light scattered into the forward hemisphere and the transmitted light to the detector. In this way opal glass takes the place of a much more expensive integrating sphere. Again, the signals both with and without the particles on the diffuser are compared. The simplicity of this technique has made it attractive to other investigators. In a modified version adapted to laser illumination (Fig. 14.2*b*), the diffusing plate method, the particle filter is both the substrate and the light diffuser (Rosen et al., 1978); it has been used to examine highly absorbing aerosols, identified as soot, from an urban environment. Rosen and Novakov (1982), in an analysis of this system, showed that backscattering by the particles does not, subject to restrictions on absorption by the filter and the particles, give rise to serious errors.

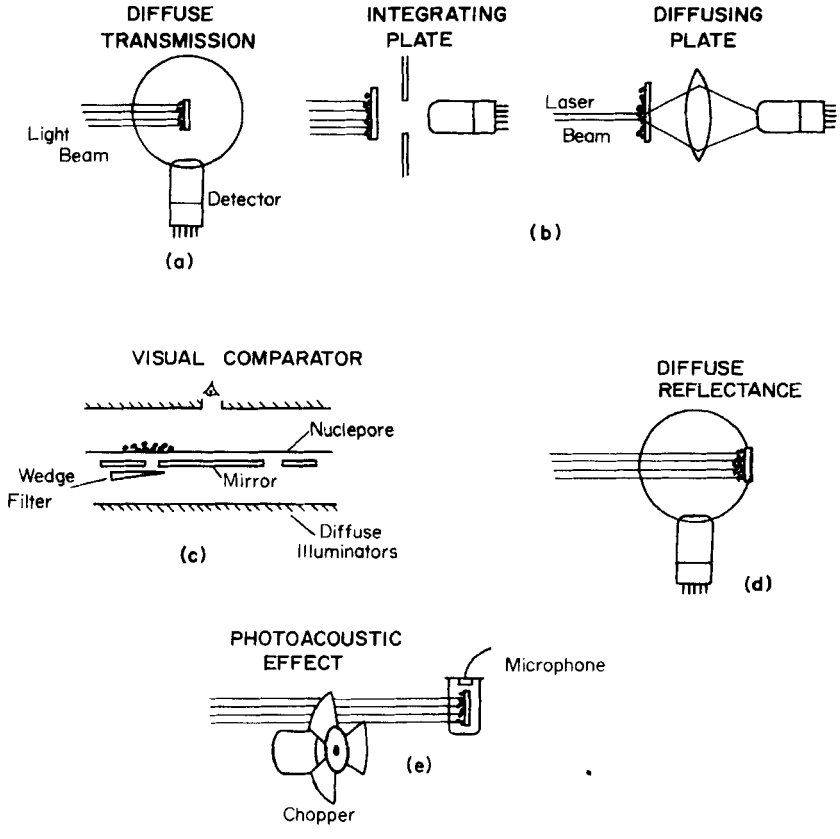

Figure 14.2 Techniques for measuring absorption by particles.

A simple scheme devised by Twomey (1980) does not even require a photoelectric detector—only the eye. A particle-laden portion of a filter and a clean portion of the same filter are each placed over holes in a thin, flat mirror, which is diffusely illuminated both from above and from below (Fig. 14.2*c*). Without the filter in place (assuming a perfect mirror) the brightness of a hole and its surroundings will be equal if the two illuminances are equal. But with the filter in place the illuminance from below will have to be reduced to obtain a brightness match, viewed from above, between a hole and its surroundings if there is any absorption. First a brightness match is obtained for the reference hole, the one over which there is only clean filter. Then a calibrated wedge filter is moved under the other hole, above which are the collected particles, until the brightness of the hole and its surroundings are matched. Knowing the wedge filter transmission, one can infer absorption by the particles.

In the diffuse reflectance technique (Fig. 14.2*d*), light scattered by a thick layer of particles is directed by the integrating sphere to a detector. Absorption

by the sample particles decreases the detector signal; the resulting diffuse reflectance spectrum is therefore qualitatively similar to the transmission spectrum of the bulk solid. This assumes, of course, that there are no shape-dependent spectral effects such as those discussed in Chaper 12; for particles of insulating solids, these are usually restricted to infrared wavelengths. To extract quantitative absorption properties of the solids, however, requires a theory of diffuse reflection; this is often the Kubelka–Munk theory (see, e.g., Kortüm, 1969). Weakly absorbing powders can be analyzed directly by this technique, but highly absorbing powders may have to be diluted in a nonabsorbing powder (Lindberg and Laude, 1974).

For completeness, we include in this brief survey a schematic diagram of the photoacoustic method (Fig. 14.2*e*), which has been discussed in Section 11.7. Absorption of chopped light by the particles gives rise to periodic heating which is detected acoustically. Scattered light does not contribute to the signal.

Good summaries of these techniques for determining absorption by collected aerosol samples are given in the proceedings of a workshop held in August 1980 (Gerber and Hindman, 1982). The participants applied their separate techniques to measuring absorption of light by particles of solids with known optical constants. Results obtained by different techniques were generally in agreement within about a factor of 5. The accuracy of k measured for carbon, which is highly absorbing, was good. But for ammonium sulfate, which is weakly absorbing, measurements consistently overestimated k by factors of 100 or more.

In the study of atmospheric aerosols several techniques have been used to determine optical constants from measurements on particulate samples. And there have been many such measurements. Yet under pressure from funding agencies and from those waiting at computer terminals for optical constants of the complicated mixture that is the atmospheric aerosol, comparatively little effort has been expended on evaluating these techniques by applying them to particles of solids with known optical constants.

14.2.5 Remote Sensing

For determining optical properties of natural aerosols remote-sensing techniques avoid some of the drawbacks of collection and measurement. Because the particles are not disturbed by collection, possible changes such as evaporation of volatile components, agglomeration, and selective losses are avoided. Remote sensing, however, has its own drawbacks. Although vertical and horizontal probing can be done to a limited extent with some of the techniques, most of them require horizontal homogeneity of the atmosphere. And the measured optical properties may not be those of most direct interest. For example, in assessing the impact of aerosols on the earth's heat balance, what is wanted is how much they absorb solar radiation and scatter it into the backward hemisphere. Of less direct relevance are the optical depth, single-scattering albedo, and asymmetry parameter. Whereas optical depth

may be determined directly, absorption must be inferred from other optical measurements, such as the extinction-to-backscatter ratio, together with a possibly oversimplified model (e.g., homogeneous, spherical particles of a single kind) the inapplicability of which may invalidate the results. Nevertheless, within limits remote sensing has excellent potential for global monitoring of some optical properties of atmospheric particles. Several remote-sensing techniques are listed below with brief comments.

Multiwavelength Solar Radiometry The sun is a light source of known spectral output. Measurement of the irradiance transmitted through the atmosphere therefore gives the total extinction from which extinction by the molecules can be subtracted to give that by the particles. Inversion techniques can then be used to infer particle size distributions from the extinction measurements (e.g., King et al., 1978). As shown in Fig. 13.8, Mie theory is a good approximation in the forward direction for sufficiently large nonspherical particles. If extinction is dominated by scattering about the forward direction, it is not very sensitive to particle shape.

Monostatic Lidar Remotely sensing atmospheric aerosols by measuring backscattering ($\theta \simeq 180°$) has become common since the ready availability of high-power pulsed lasers. Selection of various signal return times allows distance profiling. The extinction-to-backscatter ratio has been related to absorption properties of atmospheric particles using inversion techniques based on Mie theory (Spinhirne et al., 1980). It is evident from Fig. 13.8, however, that backscattering is quite sensitive to particle shape. So what is inferred as absorption perhaps should be attributed to nonsphericity. Inhomogeneity is also expected to have pronounced effects on backscattering because it is more sensitive to a particle's structure than forward scattering.

Bistatic Lidar Angular scattering by atmospheric particles can be measured by separating the collimated light source and the detector. The arrangement is much like that shown in Fig. 13.5; the volume sampled is determined by the intersection of the illuminating beam and the field of view of the detector. If a pulsed laser is used with time gating for the return signal the arrangement is called bistatic lidar. A similar system without time gating has been used for many years in searchlight probing of the atmosphere. For a survey of bistatic lidar, see Reagan et al. (1980) and references cited therein.

Linear polarization ratios have also been measured remotely. For example, results are given by Ward et al. (1973) and by Reagan et al. (1980). The sensitivity of scattering diagrams (Fig. 13.8), especially polarization (Fig. 13.9), to particle shape signals caution in inferring aerosol properties such as k from bistatic remote sensing.

14.2.6 Effective Refractive Index of Aerosols with Absorbers

The techniques just surveyed necessarily determine average refractive indices. And k values for atmospheric aerosols measured by these techniques suggest mixtures of vastly different kinds of particles. For we have noted that no

common substances have k between 0.001 and 0.01 throughout the visible; yet this is what has been inferred. There is evidence that the smaller particles are the more highly absorbing (e.g., Lindberg and Gillespie, 1977). Also, carbon in the form of soot has been identified as a component of absorbing aerosols (Rosen et al., 1978). Since k of carbon is of order 1, the implication is that the observed absorption may be attributed to a small amount of carbon mixed with much greater amounts of weakly absorbing (at visible wavelengths) substances such as ammonium sulfate, sodium chloride, and crystalline quartz. Moreover, several investigators have pointed out that the way in which the absorber is mixed with the nonabsorbers can markedly affect optical properties such as single-scattering albedo, phase, function, and backscattering cross section. Bergstrom (1973) first called attention to some of the consequences of averaging optical properties, followed by Lindberg (1975), Toon et al. (1976), Gillespie et al. (1978), and Ackerman and Toon (1981). All of the last four papers present calculations based on Mie theory to show that quantities such as the single-scattering albedo can be quite different for a given amount of absorber, depending on whether it is distributed homogeneously throughout all the particles or whether it exists as discrete particles, separate from, inside, or on the surface of, the nonabsorbers. Because different size distributions and refractive indices were used it is difficult to compare the various results. Indeed, some of them conflict, as Ackerman and Toon (1981) pointed out in mentioning their failure to reproduce a result reported previously. To gain insight, therefore, we present our own simple back-of-the-envelope calculations for the single-scattering albedo of two different models of an absorbing aerosol.

One is a mixture of 1% by particle volume of spherical absorbers with radius 0.05 μm and refractive index $m_{bl} = 1.7 + i0.7$, which is appropriate to a form of carbon, and 99% by volume of larger particles with $m_{wh} = 1.55 + i10^{-6}$, which is roughly appropriate to several possible aerosol components. The subscripts bl (black) and wh (white) indicate how separate collections of these two kinds of particles would appear. Among the many optical constants reported for carbon in its various forms we have chosen those obtained from single-sphere measurements by Pluchino et al. (1980).

The second model aerosol is composed of "gray" spheres; that is, the absorber is incorporated in the nonabsorbing particles rather than separate from them. We might visualize this as small carbon spheres uniformly embedded in plum pudding fashion throughout much larger nonabsorbing spheres.

Our first problem is how to properly calculate the average optical constants when 1% of carbon by volume is uniformly distributed in a nonabsorbing medium. The usual procedure, as in the papers cited above, has been to simply volume-average n and k separately. But optical constants are not, in general, additive, so we have used the Maxwell Garnett expression (8.50). The result is $m_{gr} = 1.55 + i0.007$, which in this instance is identical, to the number of figures shown, with the result obtained by volume-averaging the refractive indices $1.55 + i0.0$ and $1.7 + i0.7$.

We now use several approximations discussed in previous chapters to estimate for the two model aerosols their single-scattering albedo $\bar{\omega}_0$, where

$$1 - \bar{\omega}_0 = \frac{C_{\text{abs}}}{C_{\text{ext}}}.$$

For a mixture of particles, C_{abs} and C_{ext} should be interpreted as number-weighted averages.

Extinction by carbon particles of radius 0.05 μm is dominated by absorption; moreover, the absorption cross section per unit particle volume in the Rayleigh limit (12.10) is independent of radius. So taking the carbon particles to be a single size is of no consequence provided that they are sufficiently small. Q_{ext} is approximately 2 for the large nonabsorbing particles. This approximation has the advantage that it excludes the complicated ripple and interference structures of single-sphere Mie theory, which are not very realistic for broad size distributions of irregularly shaped particles (see Fig. 11.20). With these approximations, therefore, we have for the black–white mixture,

$$1 - \bar{\omega}_0 \simeq \frac{f\alpha_{\text{bl}}}{f\alpha_{\text{bl}} + (1-f)\alpha_{\text{wh}}}, \tag{14.2}$$

where the volume-normalized cross sections are

$$\alpha_{\text{bl}} \simeq 9.78\ \mu\text{m}^{-1} \quad (\lambda = 0.55\ \mu\text{m}); \qquad \alpha_{\text{wh}} \simeq \frac{1.5}{a_{\text{wh}}}.$$

To estimate $1 - \bar{\omega}_0$ for the gray particles we take $C_{\text{ext}} = 2\pi a_{\text{gr}}^2$ and use (7.2) for C_{abs}:

$$1 - \bar{\omega}_0 \simeq 0.142 a_{\text{gr}} \qquad (\lambda = 0.55\ \mu\text{m}), \tag{14.3}$$

where the factor multiplying the particle radius follows from the average refractive index $1.55 + i0.007$. The total particle volume is the same for both aerosols if $(1+f)a_{\text{wh}}^3 = (1-f)a_{\text{gr}}^3$, but a_{gr} and a_{wh} are nearly equal for $f = 0.01$.

In Fig. 14.3 we plot (14.2) and (14.3) as functions of large-particle radius. There are of course several restrictions to be kept in mind, including $2a\alpha \ll 1$ underlying the derivation of (7.2), which is only approximately satisfied for radii less than about 3 μm. To convince ardent Mie calculators that these simple expressions are approximately correct, we include single-size Mie calculations at 0.1-μm intervals. Except for the interference maxima and minima in the Mie calculations, which are unlikely to be observed in natural aerosols, the simple treatment is quite good.

The gray particles are more absorbing than the black–white mixture, and the difference is appreciable: the ratio of $1 - \bar{\omega}_0$ for the two model aerosols is

about 3. We may roughly interpret this difference as arising from two causes. First, the absorption cross section of a small carbon sphere in a medium with $n = 1.55$ is about 1.6 times that of the same sphere in air. Second, there is a focusing effect; that is, more light is geometrically incident on a sphere when it is in a much larger transparent sphere than when it is in air. For example, ignoring external and internal reflections, it follows from geometrical optics that n^2 more light is incident on a small sphere when it is at the center of a much larger sphere then when it is in air. Based on this crude reasoning, therefore, we would expect $1 - \bar{\omega}_0$ for the gray particles to be at least 1.6 times, but not more than 3.8 times, greater than that for the black–white mixture. And this is indeed consistent with more detailed calculations.

Consider now a particle radius of 1.5 μm; from Fig. 14.3 it follows that $\bar{\omega}_0$ for the gray particles is about 0.75, whereas it is about 0.9 for the black–white mixture. And recall that a single-scattering albedo of 0.85 is used widely as the critical value separating a global cooling trend ($\bar{\omega}_0 > 0.85$) from a global warming trend ($\bar{\omega}_0 < 0.85$). For particles of this size as well as those somewhat smaller and larger, therefore, even the *direction* of the temperature change depends on just how the absorber is dispersed in the aerosol. We must conclude from this, therefore, that merely knowing the amount of absorbing material in the atmospheric aerosol is not sufficient to assess its potential impact on the global climate.

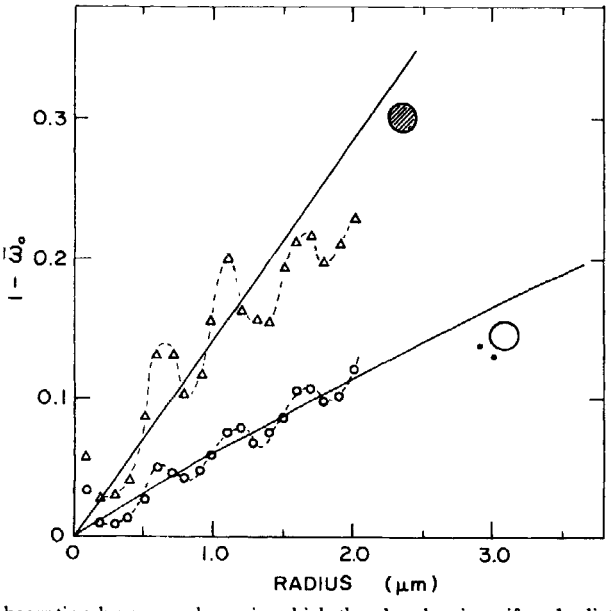

Figure 14.3 Absorption by gray spheres in which the absorber is uniformly distributed (upper) and by small absorbing spheres mixed with much larger nonabsorbing spheres (lower); the total amount of absorbing material is the same for both. Solid lines were calculated approximately and dashed lines connect points calculated with Mie theory.

14.2.7 Monitoring the Global Wind with Lidar Backscattering

It seems that we have cast atmospheric particles most often in the role of villains: they may cause cataclysmic climatic changes; they reduce visibility; they may aid in the formation of photochemical smog and acid rain. But there is a scheme afoot to make them do some useful work by acting as ubiquitous retro-reflectors for laser beams.

The Doppler shift of laser light backscattered by atmospheric particles carries information about the velocity of the air in which they are being swept along. Huffaker (1970) used a continuous CO_2 laser to demonstrate the practicability of the laser Doppler velocimeter (see Bilbro, 1980, for an overview). By using a pulsed laser and selecting signal returns at different times, particles at various distances from the source can be sampled; this is *lidar*—light detection and ranging. Doppler velocity measurements with lidar could therefore enable one to map out in direction and distance wind velocity components along the line of sight. Indeed, this concept is being considered for a future satellite-borne wind monitoring system (Abreu, 1980). As the satellite orbits the earth the infrared lidar system would scan conically looking downward into the atmosphere; depth profiling is accomplished by return-signal gating. Every chosen volume of air in the three-dimensional grid would be sampled from two different directions—forward and backward—within a short time as the satellite passes overhead. From these two line-of-sight velocity measurements the horizontal wind velocity can be extracted. Such a global wind monitoring system is quite ambitious, but would provide extremely useful meteorological data.

Small particles of some insulating solids, including those in the atmosphere, have Fröhlich modes (see Chapter 12) at certain wavelengths near 10 μm. Backscattering is also large at these wavelengths; this is evident from the efficiencies for absorption, scattering, and backscattering by a small sphere (Section 5.1), all of which contain the quantity $(m^2 - 1)/(m^2 + 2)$. Thus, the spectrum of backscattered light will peak at wavelengths near the extinction peak. Both quartz and ammonium sulfate, which are common aerosol constituents, have Fröhlich modes near 9 μm. This implies that choosing a wavelength near 9 μm rather than the more common 10.6-μm CO_2 laser radiation might give larger backscattering signals from spheres of these solids. But recall that surface modes are highly shape dependent. And backscattering should behave similarly to extinction. Figure 12.14 therefore indicates the effect of a distribution of shapes on the backscattering spectrum for quartz particles. Although CO_2 lasers are not quite tunable to the peak for quartz spheres near 9.0 μm, shape effects might actually improve the backscattering signal by spreading the spectrum of backscattered light into the region between about 9.1 and 9.2 μm where CO_2 lasers are able to operate. A Doppler lidar system operating at two different wavelengths might be able to discriminate between certain kinds of particles in the atmosphere and thus map out their distributions. But whatever use to which infrared Doppler lidar is put, it is

clear from what we have said here and elsewhere that shape-dependent surface modes in small particles will have to be reckoned with.

14.3 NOCTILUCENT CLOUDS

As their name implies, noctilucent clouds are visible at night; the sun, after it has descended well below the horizon, is their source of illumination. They are a high-latitude (50–60°) summer phenomenon and differ from clouds observed during the day by their great height, about 82 km above the earth's surface, near the height (mesopause) where the atmosphere's temperature is lowest. Tenuousness also distinguishes them from the clouds of everyday experience: stars often can be seen through them. The term "noctilucent" predates satellite observations and by now may be somewhat of a misnomer: noctilucent clouds have been observed (from a satellite) during daytime (Donahue et al., 1972). Indeed, these observations indicate that what has been seen from the ground is merely the thin and ragged edge of a much thicker high-level cloud layer extending poleward. Those of us bound to earth, however, may still use the term "noctilucent" without contradiction.

Fogle and Haurwitz (1966) have given an excellent review of noctilucent clouds, to which we refer the reader for further details about their appearance as well as when, where, and for how long they may be observed.

Probing the nature and origin of noctilucent clouds is made difficult by their inaccessibility: they are too high to be visited by balloons and too low to be visited by satellites. Rockets, therefore, are the only means for directly sampling these clouds, but rocket flights are expensive and their visits to the upper atmosphere are necessarily fleeting and restricted to small regions. Although direct sampling is, of course, highly desirable, the most practical method for investigating large regions of noctilucent clouds over relatively long time intervals is by analyzing the sunlight scattered by them or the starlight transmitted through them. Indeed, before the advent of rockets, analysis of light from noctilucent clouds was the only means of inferring their properties.

Two characteristics of the light from noctilucent clouds may be observed with no more than one's eyes and a polarizing filter: its color and whether or not it is strongly polarized. This enabled Ludlum (1957) to estimate the size range of noctilucent cloud particles. Because of the observed strong polarization he set 0.16 μm as their upper size limit; on the basis of the observed color—white, silvery, sometimes bluish, but not sufficiently so as to indicate very small particles—he set 0.008 μm as their lower size limit. From other than optical evidence he also concluded that the particles were not ice, but were more likely to be volcanic, meteoric, or interplanetary dust.

Light from noctilucent clouds carries with it more than just information about how it was scattered by cloud particles, however. On its journey from the sun to the clouds, and thence to an observer, it must travel long atmospheric paths along which it suffers selective absorption and scattering by various gases and particles of uncertain kind and amount. This selective extinction

must be subtracted from the observed spectrum to obtain the true spectrum of scattered light. Deirmendjian and Vestine (1959) corrected the spectral data of Grishin (1956) for extinction by a model atmosphere and concluded that the data were consistent with scattering by spherical particles with refractive index 1.33 and radius 0.4 μm.

14.3.1 Linear Polarization

Inferences made on the basis of the spectrum of light from noctilucent clouds are always going to be plagued by uncertainties about the corrections to be applied to ground-based observations. But the degree of polarization of light scattered by noctilucent cloud particles is insensitive to selective atmospheric extinction provided that the incident and scattered beams encounter no oriented particles (other than the noctilucent cloud particles themselves, of course). This was pointed out by Witt (1960), who measured linear polarization at scattering angles between about 20 and 60°; the degree of polarization increased monotonically with scattering angle to maximum values of about 0.4 for blue light (λ = 4900 Å) and 0.5 for red light (λ = 6100 Å). By using rockets the range of scattering angles has been extended. The high degree of linear polarization near 90° measured by Witt (1969), Tozer and Beeson (1974), and Witt et al. (1976) suggested to these authors that the upper limit of particle size is less than about 0.13 μm. Hummel and Olivero (1976) analyzed the satellite radiance measurements of Donahue et al. (1972) and concurred with this upper size limit.

The strongest evidence supporting small (< 0.1 μm) particles in noctilucent clouds is the high degree of measured linear polarization: it increases monotonically with scattering angle to almost unity near 90°. It is difficult to reconcile these observations with any conclusion other than that the particles are small.

Noctilucent cloud particles are now generally believed to be ice, although more by default—no serious competitor is still in the running—than because of direct evidence. The degree of linear polarization of visible light scattered by Rayleigh ellipsoids of ice is nearly independent of shape. This follows from (5.52) and (5.54): if the refractive index is 1.305, then $P(90°)$ is 1.0 for spheres, 0.97 for prolate spheroids, and 0.94 for oblate spheroids.

The applicability of Rayleigh-Gans theory to ice particles in the atmosphere is uncertain because $|m - 1|$ is close to values for which this theory begins to give large errors, at least for spheres (Kerker, 1969, p. 428). But if the Rayleigh–Gans theory is valid for ice particles, which requires them to be not larger than about 0.1 μm, they are necessarily highly polarizing: the degree of linear polarization at 90° is unity for all scatterers described by this theory regardless of their shape.

Some insight into how departures from Rayleigh theory affect linear polarization can be obtained from calculations of Asano and Sato (1980) for randomly oriented oblate spheroids with refractive index 1.33, which is near enough to that of ice, axial ratio $a/c = 5$, and size parameter $2\pi a/\lambda = 5$; for a

wavelength of 0.5 μm this corresponds to an equal-volume sphere with radius 0.23 μm. Polarization increases monotonically with increasing scattering angle to a maximum near 90° and then monotonically decreases. That is, polarization is similar to that for Rayleigh spheres or spheroids except that the maximum polarization (0.89) is slightly less; it is also less than that measured in the light from noctilucent clouds, which provides additional evidence that the cloud particles are not larger than about 0.1 μm.

14.3.2 Circular Polarization

Circular polarization has also been observed in light from noctilucent clouds. In a set of 10 observations Gadsden (1975) measured positive values of V/I in the range 0.02–0.07. Subsequently, Gadsden (1977) measured both positive and negative V/I; most of the values were clustered between 0 and -0.05 but a few were appreciably outside this range. The most recent measurements, however, indicate a much smaller degree of circular polarization, about 0.005 (Gadsden et al., 1979), which may be atypical or it may reflect improved measurement techniques; from this vantage point it is difficult to say which.

One possible explanation for the observed circular polarization is that noctilucent cloud particles are partially oriented, which requires that they be nonspherical. Indeed, Gadsden (1978) has criticized previous size estimates because they were made under the assumption that noctilucent cloud particles are spherical, whereas there is evidence suggesting they are not. We have shown repeatedly in previous chapters that nonspherical particles often absorb and scatter light quite differently from "equivalent" spheres. So there are certainly good reasons for carefully considering Gadsden's criticisms. Before doing so, however, it will be helpful to consider the conditions under which unpolarized light acquires a degree of circular polarization upon scattering.

For incident unpolarized light to be (partially) circularly polarized upon scattering by a collection of particles, the scattering matrix element S_{41} must not be zero. It was shown in Section 13.6 that the scattering matrix for a collection (with mirror symmetry) of randomly oriented particles has the form

$$\begin{pmatrix} S_{11} & S_{12} & 0 & 0 \\ S_{12} & S_{22} & 0 & 0 \\ 0 & 0 & S_{33} & S_{34} \\ 0 & 0 & -S_{34} & S_{44} \end{pmatrix}. \tag{14.4}$$

If each particle is spherically symmetric, then $S_{33} = S_{44}$ and $S_{11} = S_{22}$. Such a collection of particles cannot circularly polarize unpolarized light or light polarized perpendicular (or parallel) to the scattering plane. But it can circularly polarize *obliquely* polarized incident light ($U_i \neq 0$) provided that S_{43} ($-S_{34}$) is not zero.

According to the ground rules laid down at the beginning of this book, multiple scattering is excluded from consideration. But it is not always prudent to pretend that multiple scattering does not exist. Fortunately, it is almost trivial—the mathematical apparatus of radiative transfer theory is unnecessary—to extend our treatment of scattering and circular polarization to multiple scattering media, and in this instance it is worth the small amount of effort required to do so.

Consider a particulate medium described by (14.4); for ease of visualization it may be taken to be a single particle. Unpolarized light will, upon scattering, become partially polarized either parallel or perpendicular to the scattering plane depending on the sign of S_{12}. This scattered light is now incident on another particle, but it is polarized obliquely, in general, to the various scattering planes determined by the directions of single-scattered (i.e., incident) and twice-scattered light. So unpolarized light can acquire a degree of circular polarization upon multiple scattering by randomly oriented particles.

Particles to which the Rayleigh–Gans theory is applicable, regardless of their shape, orientation, and composition, do not circularly polarize either unpolarized or linearly polarized light upon scattering, single or multiple, because $S_{41} = S_{42} = S_{43} = 0$. This is also true of *nonabsorbing* particles in the Rayleigh limit (Chapter 5), which follows from (3.16) and (5.47): the polarizability tensor is real. Ice is weakly absorbing at visible wavelengths (Grenfell and Perovich, 1981). Within the framework of both the Rayleigh and the Rayleigh–Gans theories, therefore, ice particles, regardless of their shape and orientation, cannot circularly polarize unpolarized or linearly polarized visible light.

We are still left with the question of the origin of the observed circular polarization of light from noctilucent clouds. Circular polarization of *unpolarized* incident light is possible if the cloud particles are appreciably larger than allowed by Rayleigh theory—provided that they are aligned. But no plausible alignment mechanism has yet been proposed. Gadsden (1975) suggested aerodynamic alignment, but this mechanism does not stand close examination: aerodynamic forces are very weak in the thin atmosphere at 82 km above the earth's surface. Moreover, whether or not elongated particles are aligned by falling in air is not independent of their size: alignment is counteracted by the disorienting tendency of Brownian rotation. Fraser (1979) has shown that, at sea level, the critical size below which particles are randomly oriented is about 10 μm. The critical size is not very sensitive to temperature and pressure, but it does increase slightly with altitude. Extrapolation from sea level to the mesopause where the mean free path of molecules is about 0.5 cm is, in general, invalid. But in this instance the critical size increases even faster than predicted by extrapolating Fraser's results. Indeed, Reid (1975) has calculated the force on an arbitrarily shaped particle, small compared with the mean free path (molecular flow regime), from which it follows that the net couple acting on such a particle is zero. Until an alignment mechanism is discovered, therefore, we can only assume that noctilucent cloud particles are

randomly oriented and thus incapable of circularly polarizing unpolarized light.

A possible explanation for the observed circular polarization is that the light illuminating noctilucent clouds is partially polarized because of multiple scattering in the long paths it travels through the atmosphere. The incident light is therefore composed of unscattered, unpolarized (direct) light and multiply scattered, partially polarized (indirect) light:

$$\begin{pmatrix} I_i \\ Q_i \\ U_i \\ V_i \end{pmatrix} = \begin{pmatrix} I_0 \\ 0 \\ 0 \\ 0 \end{pmatrix} + \begin{pmatrix} I_{\text{ms}} \\ Q_{\text{ms}} \\ U_{\text{ms}} \\ V_{\text{ms}} \end{pmatrix}$$

incident	unscattered sunlight (direct)	multiply scattered sunlight (indirect)

If such light is incident on a medium described by the matrix (14.4), the degree of circular polarization of the scattered light is

$$\frac{V_s}{I_s} = \frac{-\dfrac{S_{34}}{S_{11}}\dfrac{U_{\text{ms}}}{I_{\text{ms}}} + \dfrac{S_{44}}{S_{11}}\dfrac{V_{\text{ms}}}{I_{\text{ms}}}}{\dfrac{I_0}{I_{\text{ms}}} + 1 + \dfrac{S_{12}}{S_{11}}\dfrac{Q_{\text{ms}}}{I_{\text{ms}}}}. \tag{14.5}$$

Note that the direct light is scattered through a single angle to an observer, whereas the indirect light, which is incident from many directions, is scattered through many angles; so S_{34}/S_{11}, $U_{\text{ms}}/I_{\text{ms}}$, and so on, should be interpreted as averages over the various directions of incidence.

If V_s/I_s is to be nonzero, either S_{34}/S_{11} and $U_{\text{ms}}/I_{\text{ms}}$, or S_{44}/S_{11} and $V_{\text{ms}}/I_{\text{ms}}$, or both, must not be zero. S_{34} is zero for nonabsorbing particles in the Rayleigh limit and for arbitrary particles in the Rayleigh–Gans approximation. Even for particles—spherical and nonspherical—of size comparable with the wavelength, however, S_{34} tends to be small, particularly in the forward direction (see Figs. 13.13 and 13.14).

If we neglect the product $(S_{34}/S_{11})(U_{\text{ms}}/I_{\text{ms}})$, then the degree of circular polarization of the scattered light is approximately

$$\frac{V_s}{I_s} \simeq \frac{I_{\text{ms}}}{I_0}\frac{S_{44}}{S_{11}}\frac{V_{\text{ms}}}{I_{\text{ms}}},$$

where we have also assumed that I_0/I_{ms} is the dominant term in the denominator of (14.5).

A necessary condition for the correctness of the multiple-scattering explanation of the observed circular polarization is that scattering by noctilucent cloud particles does not appreciably reduce the degree of circular polarization of the incident light. That this is so for randomly oriented Rayleigh ellipsoids is readily shown. M in (5.52) is nearly unity for ice ellipsoids, so to good approximation

$$\frac{S_{44}}{S_{11}} \simeq \frac{2\cos\theta}{1+\cos^2\theta},$$

which is not less than 0.5 except for a small range of scattering angles centered about 90°.

It is required further that V_{ms}/I_{ms} be not smaller than the observed values of V_s/I_s; indeed, it should be a good bit larger because of the dilution factor I_{ms}/I_0. Gambling and Billard (1967) measured degrees of circular polarization as high as 0.67 in light from cloudless skies, although more typically they ranged between 0 and 0.17. These values may be taken to represent fairly the degree of circular polarization expected in the multiply scattered light illuminating noctilucent clouds.

Both V_{ms}/I_{ms} and I_{ms}/I_0 must be about 0.2 or higher if the highest values of circular polarization are the result of multiple scattering; if they both are about 0.07, the multiple scattering explanation is consistent with the lowest observed values. To put it another way, V_{ms}/I_0 must be not less than the observed degree of circular polarization; this is at least plausible—there are no strong reasons for rejecting it—but it has yet to be demonstrated unequivocally.

14.3.3 Summary

The high degree of linear polarization observed in light from noctilucent clouds strongly suggests that the particles cannot be much larger than about 0.1 μm. And if they are composed of ice, they need not be spherical. Regardless of their shape and orientation, small ice particles do not circularly polarize unpolarized light.

Aligned, hence nonspherical, particles have been suggested as the cause of the observed circular polarization in light from noctilucent clouds. But no plausible alignment mechanism has yet been proposed. Even if a mechanism were to be discovered, however, it is likely that the size required for alignment would not be consistent with the linear polarization data: particles are aligned by a couple—a force times a distance. Whatever the mechanism, therefore, alignment favors larger particles.

There are several possible explanations for the circular polarization data: they are in error; the particles are small, aligned, and highly absorbing; the light illuminating the clouds has acquired a degree of circular polarization by multiple scattering.

There is no reason for suspecting the data; we must take them at face value.

If the particles are highly absorbing, it may be difficult to reconcile this with both the observed color and linear polarization of the light from noctilucent clouds.

The third explanation is the most likely one, although further measurements and calculations are necessary to establish this with reasonable certainty. In the context of the multiple scattering explanation a statement by Witt et al. (1976) is apposite: "Although multiple scattering effects within the mesosphere itself need not be considered, the additional source of light from the lower atmosphere must be fully taken into account to allow the proper interpretation of upper-atmospheric polarization measurements."

14.4 RAINFALL MEASUREMENTS WITH RADAR

The ever-increasing number of papers presented at the radar meteorology conferences sponsored by the American Meteorological Society attest to the rapidly growing use of radar in meteorology; indeed, the collection of preprints will soon be beyond the ability of one person to lift, let alone read. To cover the various applications of radar meteorology adequately therefore requires more space than we can devote here. A more complete survey of the field is given in the standard work on radar meteorology by Battan (1973). More recently, Browning (1978) reviewed several applications of radar to meteorology, from which we have chosen one for discussion: measurement of rainfall by radar. A review of this topic is given by Wilson and Brandes (1979).

Let us assume for the moment that all raindrops have the same diameter D. The rainfall rate R, the rate at which the depth of water in a rain gauge of constant cross section increases with time, is the product of the total volume of water in a unit volume of air and the terminal velocity $V_t(D)$ of a raindrop:

$$R = N\frac{\pi}{6}D^3V_t(D),$$

where N is the number of raindrops per unit volume of air. It is sometimes overlooked that V_t is the velocity *relative to the ground*, whereas various theoretical and empirical expressions are for terminal velocities *relative to the air* through which the droplet falls (Battan, 1976). If the raindrops were to fall in an updraft with velocity V_t, for example, the rainfall rate would be zero.

In principle the rainfall rate is determined by two quantities, the amount of water in the air and the rate at which it is falling to the ground. But these two quantities are correlated to some extent: V_t increases with increasing D as does, for a given N, the amount of water. Yet this correlation has not been established precisely. So it is perhaps best to assume that determining rainfall rates requires two independent measurements.

Raindrops, which have diameters in the range 1–5 mm, are small compared with the wavelengths of weather radars, usually 3, 5, or 10 cm. We showed in Section 5.1 that the backscattering cross section of a sphere is proportional to

the sixth power of its radius in the Rayleigh approximation. So it is customary to define the *radar reflectivity factor*

$$Z = ND^6,$$

which determines the amount of power scattered by raindrops in a unit volume at a given distance back to a receiving antenna.

When a raindrop ceases to accelerate, its weight is balanced by the drag force (buoyancy is negligible):

$$\rho_w \frac{\pi}{6} D^3 g = \frac{1}{2} \rho_a V_t^2 C_d \frac{\pi}{4} D^2,$$

where ρ_a and ρ_w are the densities of air and water, g is the acceleration of gravity, and C_d is the drag coefficient. The drag coefficient of a raindrop is nearly independent of its diameter (Gunn and Kinzer, 1949), in which instance its terminal velocity is approximately proportional to the square root of its diameter.

If all these results are combined we obtain the following Z–R relation:

$$Z = KN^{-0.71} R^{1.71},$$

where K is a constant. Thus, there is a unique relation between the radar reflectivity factor and the rainfall rate provided that N is constant, or nearly so, from storm to storm, and all droplets are the same size. A Z–R relation puts the cart before the horse, however, for it is the rainfall rate that is to be determined by measuring the reflectivity factor, not the converse. Nevertheless, this is the convention, hallowed more by tradition than by ratiocination.

Up to this point we have assumed for simplicity that all raindrops are the same size. A more realistic assumption is that raindrop diameters are distributed according to a continuous function $N(D)$, in which instance the radar reflectivity factor and the rainfall rate are

$$Z = \int N(D) D^6 \, dD, \qquad R = \frac{\pi}{6} \int N(D) V_t(D) D^3 \, dD.$$

It has become the custom to express Z–R relations in the form

$$Z = aR^b,$$

where a and b are constants. They may be constant as far as individual investigators are concerned but among them there is no consensus: reported pairs of values of a and b differ in varying degree. Twomey (1953) lists eight different Z–R relations and adds one of his own to the pile; Battan (1973, pp. 90–92) lists nearly 70 different Z–R relations. Each year sees a new crop—and the end is not yet in sight.

With Z–R relations having been steadily churned out for nearly 40 years, it is only natural to ask: How good are they for determining rainfall rates? Twomey (1953) concluded that "radar methods can give only an approximate measure of precipitation rate; the value deduced from the radar echo may be in error by a factor of 2 : 1 either way, and this randomly distributed error is independent of instrumentation or procedure adopted." With these words in mind it is indeed sobering to contemplate the latest word on Z–R relations in the review article by Wilson and Brandes (1979): "With reasonable efforts, radar measurements... should be within a factor of two of the true rainfall about 75% of the time." In other words, not much progress has been made in over a quarter of a century. One cannot help feeling that this results from a failure to come to grips with a fundamental constraint imposed by nature: it really requires *two* independent measurements to determine rainfall with radar and no amount of statistical manipulation will ever change this.

We have assumed in previous paragraphs that raindrops are spherical, although this is not generally their shape. Nor are they shaped like teardrops despite the nearly universal habit of artists to so depict them. Their actual shape may be quite complicated; moreover, they oscillate, so the notion of a single shape for a raindrop is somewhat of an idealization. Sufficiently large raindrops are approximately spheroidal (oblate): they are flattened in the direction of fall. The forces shaping raindrops have been discussed by McDonald (1954). More recent treatments of raindrop shape are those by Pruppacher and Pitter (1971) and Green (1975). In the former there is a curve (Fig. 3) showing that the amount of deformation of a drop increases with its size. But so does its terminal velocity, which in turn implies that the deformation depends on the droplet velocity.

Radar backscattering by spheres is independent of the polarization state of the beam. But backscattering by spheroids (excluding illumination along their symmetry axes) is not. This is the physical basis for a method proposed by Seliga and Bringi (1976) for improving rainfall measurements by measuring two radar reflectivities, denoted by Z_H (horizontal polarization) and Z_V (vertical polarization), for orthogonally polarized beams. Ratios of the amount of radiation (singly) scattered for various polarization states of the incident beam are independent of the number of particles. As a consequence, the *differential reflectivity* Z_{DR}, defined by

$$Z_{\mathrm{DR}} = 10 \log \frac{Z_H}{Z_V},$$

depends only on a mean size of the drops; Z_{DR} is zero, of course, if they are spheres. With this mean size and either Z_H or Z_V, the number of particles can be determined. So the two quantities necessary to determine rainfall rates, number and size, can be obtained in principle from the two reflectivity measurements.

The first tests of this proposed method have been encouraging. On the basis of comparisons between rainfall rates measured with the differential reflectivity technique and with a network of rain gauges, Seliga et al. (1981) concluded that "these first measurements of rainfall using the Z_{DR} technique support the theoretical expectations... that rainfall rate measurements with radar can be made with good accuracy." So it may yet be possible to accurately measure rainfall with radar—provided that measurements are made with two orthogonally polarized beams. This exemplifies one of the principal themes of this book: scattered polarized radiation contains information that may be put to good use.

14.5 INTERSTELLAR DUST

Interstellar dust, the small particles sparsely populating the regions between stars, has probably been studied as much as or more than any system of particles on earth, either laboratory produced or naturally occurring. Serious scientific study of interstellar dust has been going on since the early part of this century, and according to one of the latest review articles (Savage and Mathis, 1979), about 300 research papers that are in some way related to interstellar dust are being published yearly. Other review articles that survey this field and provide guides to its extensive literature are those of Wickramasinghe and Nandy (1972), Aannestad and Purcell (1973), and Huffman (1977); the monograph by Martin (1978) also covers the field well.

Advances in several areas of physics have followed from astronomical observations. Examples may be found in atomic spectroscopy, high-energy particle physics, and relativity. Even for optical studies of small particles the "cosmic laboratory" may have some advantages over laboratories bound to earth. We noted in Section 12.2 how difficult it is to produce submicrometer particles and to prevent them from aggregating; and it may also be necessary to maintain them in a high-vacuum environment while their absorption and scattering properties are being determined. But these requirements are admirably met by interstellar dust, which astronomers have studied carefully at wavelengths from far infrared to far ultraviolet and even x-rays.

The consequences of interstellar dust may be seen with the unaided eye. Under good seeing conditions dark patches can be observed in the Milky Way. These dark areas, we now know, do not result from the irregular distribution of stars in our galaxy but rather from the very effective obscuration of starlight by irregular clouds of small particles, the interstellar dust.

Several different types of this dust are distinguished by astronomers. On average, interstellar dust resides in widely separated *diffuse clouds*. But there are also dense regions of gas and dust into which little ultraviolet radiation can penetrate, thereby providing an environment for the formation of complex molecules; these are referred to as *molecular clouds*. Clouds of particles expelled by cooler stars into the regions around them are called *circumstellar*

shells. Other dusty interstellar regions are found around novae, planetary nebulae, and in diffuse nebulae.

If all the matter in our galaxy, which is about evenly divided between the stars and the regions between them, were uniformly distributed, its average density would be about 6×10^{-24} g/cm^3. The solid component of the interstellar medium composes about 5% of its mass. But despite its low average density—about 1.5×10^{-26} g/cm^3—interstellar dust has an important effect on the distribution of electromagnetic radiation in our galaxy.

14.5.1 Extinction

The effectiveness of interstellar dust at extinguishing starlight is illustrated by the following example. If a kiloparsec (3.3×10^3 light years) column of dust were compressed into a homogeneous solid with a density of 2 g/cm^3, its thickness would be about 0.2 μm. Yet this small amount of dust transmits only about 6% of the visible light incident on it.

A great amount of effort has been expended on measuring the spectral dependence of interstellar extinction. Unlike laboratory samples, interstellar dust cannot be placed in and then taken out of a light beam, so astronomers must rely on finding two separate but similar light sources. These are two stars of similar spectral type, as judged by their emission spectra, but selected so that one has a large amount and the other a small amount of dust between it and the observer. Comparison of the light from the reddened star (I)—so named because its light is selectively depleted of longer wavelengths by extinction—with that from the unreddened star (I_0) enables the optical density $\log_{10}(I_0/I)$ to be determined.

The average interstellar extinction spectrum, which may not be representative of localized galactic regions, for a path length of 1 kiloparsec is shown in Fig. 14.4.

Extinction of visible light increases almost linearly with increasing photon energy (decreasing wavelength); interstellar dust, like the molecular and particulate constituents of our atmosphere, reddens starlight by extinction. Although this does not shed much light on the composition of the dust, it does imply that most of the particles responsible for interstellar extinction are small compared with visible wavelengths. Other features of the extinction spectrum are a prominent broad peak at about 5.7 eV (2170 Å)—referred to as the 2200-Å band—beyond which extinction continues to rise, and a less conspicuous knee in the curve near 2.8 eV (4500 Å).

Most explanations of the interstellar extinction curve, which are based on calculations for spherical particles (e.g., Mathis et al., 1977), require several different dust components: a special substance to give the 2200-Å band; very small particles for the far-ultraviolet upturn; and a larger size component to redden visible light. That very small spheres are needed for rising ultraviolet extinction is evident from Figs. 4.6 and 11.2. Particles of the proper size to match interstellar reddening in the visible would generally give rather neutral

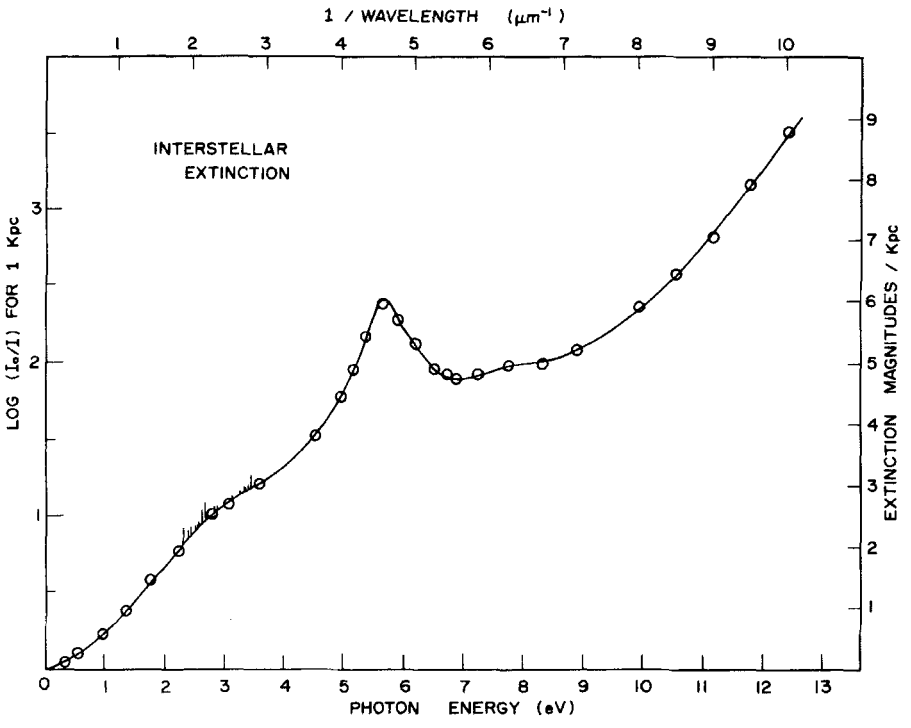

Figure 14.4 The average interstellar extinction spectrum. Data points are from Savage and Mathis (1979).

extinction at much shorter wavelengths: hence the apparent need for very small particles so that extinction continues to rise at these wavelengths. But there are laboratory measurements for graphite particles which suggest that the small-particle component may not be necessary (Day and Huffman, 1973).

Superimposed on the smoothly varying interstellar extinction curve is a series of some 39 or more narrow extinction bands ranging in width from a few angstroms to about 30 Å (Herbig, 1975; Snow et al., 1977). Although much is known about these bands—their positions, shapes, and relative strengths—not one of them has been satisfactorily explained. Because of their large widths compared with atomic and molecular absorption bands, astronomers call them the *diffuse* bands, although they are quite narrow compared with absorption bands in solids. The strongest band, near 4430 Å, was discovered between 1910 and 1920 and determined in the 1930s to be of interstellar origin. Since then the list of bands has continued to grow, with the spectroscopic information becoming ever better, yet with little definite progress in explaining their origins. At present the diffuse band mystery must surely be the most outstanding unsolved spectroscopic problem in astronomy, ranking with the longest-standing such problems of the last two centuries. The solution to this mystery

is likely to elucidate greatly the nature of the interstellar medium and may lead to a major new investigative probe for astronomers.

Of more recent discovery are wide and shallow extinction bands with characteristic widths of about 500–1000 Å and extending from about 3400 to 11,000 Å (for a brief survey, see Huffman, 1977). This very broad structure (VBS) is too broad and weak to be seen in Fig. 14.4. Lack of correlation between the diffuse bands and the VBS suggests a different origin for the two.

14.5.2 The 2200-Å Band

Clearly, the dominant feature in the ultraviolet is the prominent peak near 2200 Å. This strong and generally occurring feature has increased the number of specific suggestions for the composition of interstellar dust beyond that possible if only reddening of visible light were known. The most widely held interpretation of this feature is that it is the result of extinction by small graphite particles, which, as pointed out by Gilra (1972ab), have a surface plasmon oscillation in the ultraviolet. Both Mie calculations using measured bulk optical constants of graphite and laboratory measurements (Day and Huffman, 1973; Stephens, 1980) have demonstrated the surface plasmon peak in small graphite particles, although neither agrees completely with the exact shape and position of the interstellar feature. In common with other such collective oscillations, discussed extensively in Chapter 12, the graphite feature might be expected to be quite sensitive to particle shape. But extinction by small graphite particles is not nearly as dependent on shape as that by small metallic (free electron) particles. We showed in Section 12.4 that the surface plasmon peak for aluminum particles can lie anywhere below the plasma frequency, which is in the ultraviolet, because this is the spectral region over which ϵ' for aluminum is negative. But for graphite there is only a relatively narrow range (4–7 eV) over which one of the principal components of its dielectric tensor is negative. Particle shape can thus be important but only within a restricted spectral region. Departures from sphericity may shift and broaden the sphere feature somewhat but they do not completely obliterate it. In this sense the extinction feature in small graphite particles, although the result of a collective electronic oscillation (surface plasmon), more nearly resembles collective lattice oscillations (surface phonons) in insulating particles such as quartz, silicon carbide, and MgO, for which the negative ϵ' region is relatively narrow (see Chapter 12).

There are several possible reasons why neither calculations nor measurements of graphite extinction agree in detail with the observed interstellar band. Calculations require accurate values of both sets of optical constants for graphite, which is highly anisotropic. But there are very large discrepancies among different measured optical constants for the experimentally difficult case when the electric field is parallel to the optic axis. Moreover, the optical constants of graphite depend on its degree of crystallinity. These factors have been discussed in the review by Huffman (1977). Even with accurate optical

constants, however, the scheme for calculating extinction by anisotropic spherical particles (see Section 8.2) is of uncertain validity outside the Rayleigh limit. Finally, because graphite is anisotropic, particles of it are likely to be nonspherical, and nonsphericity is difficult to treat outside the Rayleigh limit. For these reasons failure to match the observed 2200-Å band with either calculations or measurements is perhaps not too surprising. Other explanations, of course, have been proffered; these are discussed in the articles cited in the first paragraph of this section.

14.5.3 Infrared Absorption Bands

Interstellar extinction features become increasingly difficult to observe as the wavelength is extended farther into the infrared because the cross section decreases, necessitating extremely long path lengths through the dust, while emission from heated dust around stars opposes absorption, filling in absorption bands and complicating interpretation. One of the best places to look for infrared absorption bands—absorption is nearly synonymous with extinction at infrared wavelengths if the particles are sufficiently small, say < 0.1 μm—is toward the center of the galaxy: the large concentration of stars near the galactic center and the long path lengths are favorable to detecting weaker absorption bands. The intensity spectrum in the direction of the galactic center shows a prominent absorption band at 9.7 μm (see Fig. 3 in Woolf, 1975, which is reproduced as Fig. 12 in Huffman, 1977). This band, although generally difficult to observe in interstellar extinction, has been observed as an excess emission hump in a variety of astronomical sources, including circumstellar shells, diffuse nebulae, and comet tails.

Soon after its discovery the broad and featureless 9.7-μm band was associated with Si—O vibrational stretching modes in silicates such as the mineral olivine $(Mg, Fe)_2SiO_4$. But when the optical constants of olivine were measured and extinction calculations performed it was evident that, in contrast with the observed structureless band, sharp structure would persist even for a distribution of particle sizes and shapes: there are several regions where ϵ' is negative, but sufficiently isolated from one another that shape does not cause the corresponding bands to overlap appreciably. Suggestions that disordering the crystal lattice would broaden such bands were confirmed by measurements of optical constants of highly disordered silicates together with small-particle extinction calculations and measurements (Day, 1976; Krätschmer and Huffman, 1979). This work shows that highly disordered silicates fit the featureless 9.7-μm interstellar band quite well. Absorption bands in disordered silicates are sufficiently weak compared with those in ionic solids that shape effects, such as those dominating the spectra discussed in Section 12.3, are not very important.

Although the 9.7-μm band is difficult to observe in typical interstellar regions, it has been found in the spectra of astronomical objects embedded in dense molecular clouds. Also commonly found in such clouds is an absorption

band at 3.07 μm, usually attributed to ice, both water and ammonia. In water ice the band corresponds to the O—H stretching mode (see Section 10.3). Water was once thought to be a major component of the interstellar dust, but failure to detect a strong 3.1-μm ice band has somewhat weakened this view. The ratio of strengths of the 3.07- and 9.7-μm bands in molecular clouds varies widely, strongly suggesting that different substances are responsible for the two features. It may be that silicate grains become coated with a mantle of ice in the more protected regions of molecular clouds. To calculate extinction by such coated particles—assuming they are spherical—requires the theory of Section 8.1 and Appendix B; examples of such calculations are given by Aannestad (1975).

14.5.4 Emission Spectra of Circumstellar Shells

Stars further along in their life cycle are often cooler and redder than younger stars. Shells of dust that has been condensed from material ejected from these cool stars often surround them. Such circumstellar dust shells, heated by the stars, emit strongly in the infrared with a spectrum characteristic of absorption bands in the dust: the emissivity of a small particle is equal to its absorption efficiency (see Section 4.7). An excellent review of circumstellar dust has been given by Ney (1977).

Critical to the composition of the condensate is the carbon-to-oxygen ratio in the star. If carbon dominates (C/O > 1), the oxygen is tied up in gaseous carbon compounds, leaving excess carbon to combine with other elements to form solids. Probable condensation products of such carbon stars are SiC and solid carbon, perhaps in the form of graphite, amorphous carbon, or some intermediate structure. If the star is oxygen rich (C/O < 1), condensation is dominated by excess oxygen left over when the carbon is depleted, leading to probable solids such as oxides, including the silicates.

Two emission spectra of circumstellar shells are shown in Fig. 14.5, for an oxygen star in the bottom part of the figure and for a carbon star in the top.

Rising above the background emission, assumed to be that of a blackbody at 3000°K, is a broad 9.7-μm feature for the oxygen star. Between about 15 and 20 μm a much weaker excess emission feature is also evident. A measured absorption spectrum of amorphous olivine smoke particles (Krätschmer and Huffman, 1979) is shown for comparison.

Dust around the carbon star shows an excess emission feature between about 10.2 and 11.6 μm, clearly distinguishable in both shape and position from the 9.7-μm feature of the oxygen star, which has been attributed to small SiC particles. These particles cannot be spherical, however. According to the discussion in Section 12.2, shape effects spread an absorption band in small particles of materials like SiC between the transverse (ω_t) and longitudinal (ω_l) optical mode frequencies; these frequencies for SiC are indicated on the figure. This point was made by Treffers and Cohen (1974) using Gilra's unpublished calculations. To illustrate this further, calculations for a random distribution of

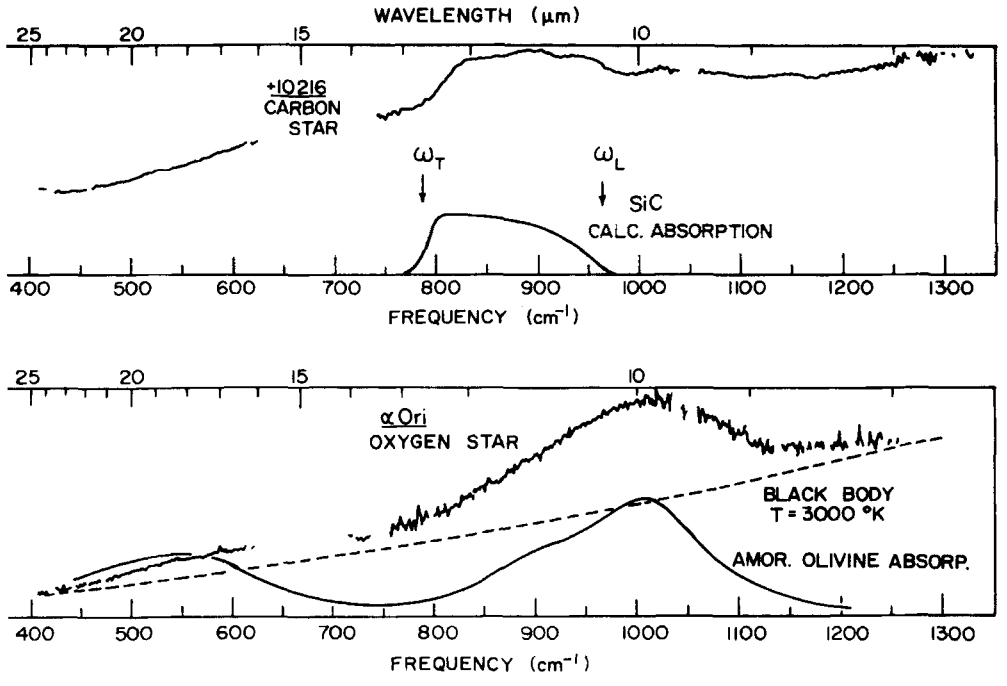

Figure 14.5 Emission spectra of dust shells around a carbon star (top) and around an oxygen star (bottom). From Treffers and Cohen (1974).

Rayleigh ellipsoids, arbitrarily normalized, are reproduced from Fig. 12.15. Spherical SiC particles match the circumstellar feature very poorly, but a wide distribution of shapes matches it quite well. This indicates that even shape information may sometimes be extracted from emission spectra of inaccessible particles.

14.5.5 Linear Polarization

Interstellar dust partially polarizes, as well as attenuates, the light it transmits, which places further constraints on particle size and composition. It is almost certain that this polarization is caused by asymmetric particles aligned in the galactic magnetic field, although the exact alignment mechanism is still uncertain (Aannestad and Purcell, 1973). The degree of linear polarization is as much as 10% and peaks between 0.4 and 0.8 μm. Although both the maximum polarization P_{max} and the corresponding wavelength λ_{max} vary from star to star, the normalized polarization P/P_{max} falls on a single curve (Fig. 14.6) when plotted against normalized wavelength λ_{max}/λ (Coyne et al., 1974). According to Martin (1974) this scaling relation implies that the optical constants of the particles at and near visible wavelengths do not vary apprecia-

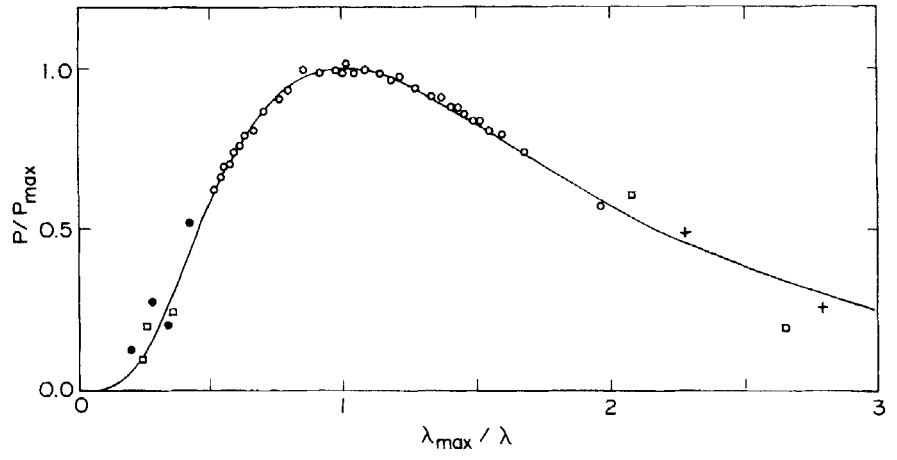

Figure 14.6 Observed linear polarization of light from several stars; λ_{max} is the wavelength at which the maximum polarization P_{max} occurs. From Coyne et al. (1974).

bly. This is evidence against graphite and in favor of insulating solids such as silicates, ices, SiC, etc. There does not appear to be a polarization feature associated with the 2200-Å extinction band generally attributed to graphite (Gehrels, 1974b); this indicates that the particles responsible for this band are not aligned.

Unpolarized incident light is partially polarized upon extinction by particles if the cross section depends on polarization; the degree of linear polarization is proportional to the difference in the cross sections for light polarized in two orthogonal directions. Aligned cylinders (Fig. 8.7) and aligned spheroids (Fig. 11.16) are examples of such particles. Note in Fig. 11.16 that the difference between the two cross sections for the oblate spheroid ($\zeta = 30°$) is greatest on the steeply rising part of the extinction curve. For a given particle size the degree of polarization is least for the smaller size parameters (longer wavelengths), increases with decreasing wavelength to a maximum, then decreases, and eventually reverses sign. If the particle size is increased, the polarization maximum shifts to a longer wavelength; if it is decreased, the maximum shifts to a shorter wavelength. Although the wavelength of maximum polarization depends on size, the degree of polarization depends on only the *ratio* of size to wavelength—provided that the optical constants vary weakly over the wavelength range of interest. This helps to explain Fig. 14.6.

14.5.6 Circular Polarization

Small degrees of circular polarization (V/I) in starlight, usually less than 1%, have been observed in recent years; the polarization modulation technique for observing such polarization was discussed in Section 13.7. There are at least two mechanisms for circularly polarizing starlight.

An interstellar dust cloud containing aligned particles may be looked upon as a linearly birefringent (and possibly linearly dichroic) medium (van de Hulst, 1957, p. 58): the cloud acts like a retarder. We showed at the end of Section 2.11 that linearly polarized light becomes circularly polarized upon transmission by a retarder. The first clear evidence for this kind of polarization mechanism was reported by Martin (1972), where light from the Crab Nebula was the source of linearly polarized incident light.

Interstellar grains may also circularly polarize unpolarized light. Such light is partially linearly polarized upon traversing a cloud of aligned grains. If this linearly polarized light is then incident on another cloud of aligned grains, where the alignment axis of the second set of grains is rotated relative to that of the first, the transmitted light will be partially circularly polarized. This is the simplest example of grain alignment changing along the line of sight, a mechanism for circular polarization discussed in detail by Martin (1974). A certain amount of this type of changing alignment is expected to be fairly common and provides the accepted explanation for the small degrees of circular polarization observed in light from a number of stars.

14.5.7 Scattering by Interstellar Dust

Light scattered by interstellar dust carries with it information about the grains. Such scattered light has been observed as diffuse galactic light (DGL), the faint but general glow of scattered starlight, and as reflection nebulae, the scattered light from particularly dense clouds of dust near bright stars or groups of stars. Diffuse galactic light is very weak compared with other sources of sky brightness, such as direct starlight, the zodiacal light from interplanetary dust in our solar system, and atmospheric airglow. But in spite of this, measurements of DGL together with extinction give the best values of the ratio of scattering to extinction—the single-scattering albedo—by interstellar grains. Reflection nebulae, like the one around the star Merope in the Pleiades and the large bright area in the constellation Orion, are much brighter than diffuse galactic light. Unfortunately, the configuration of source and dust is often poorly known. Even with the source of illumination in front of the dust cloud—perhaps the best configuration from the point of view of interpreting observations—it has been difficult to fit both angular intensity and polarization measurements with Mie calculations. Zellner (1973) concluded from this that Mie theory may be inapplicable to particles in reflection nebulae. In this connection refer to the discussion of scattering by nonspherical particles in Section 13.4, particularly Figs. 13.8 and 13.9. Recall that polarization by nonspherical particles can be opposite in sign to that by equivalent spheres of the same material (Fig. 13.9). And disagreement between the measured angular distribution of scattered light and that calculated by Mie theory (Fig. 13.8) is greatest in the backward directions; but these are the directions of light from reflection nebulae with the simplest configuration.

Extracting information about interstellar dust from analysis of scattered light, as opposed to transmitted light, is fraught with many difficulties.

14.5.8 Far-Infrared Emission

It is not difficult to show that the emissivity of small spherical particles, composed of both insulating and metallic crystalline solids, is expected to vary as $1/\lambda^2$ in the far infrared. For example, if the low-frequency limit of the dielectric function for a single Lorentz oscillator (9.16) is combined with (5.11), the resulting emissivity is

$$e = Q_{\text{abs}} \simeq \frac{48\pi^2 ac}{(\epsilon_0 + 2)^2} \frac{\gamma\omega_p^2}{\omega_0^4} \frac{1}{\lambda^2} \qquad (\omega \ll \omega_0)$$

where a is the sphere radius, c is the speed of light *in vacuo*, and $\epsilon_0 = \epsilon'(0)$. In this instance, therefore, the emissivity varies as $1/\lambda^2$ at frequencies well below the resonant frequency ω_0. Similarly, for a small metallic sphere with the Drude dielectric function (9.27), we have

$$e \simeq \frac{48\pi^2 ac\gamma}{\omega_p^2} \frac{1}{\lambda^2} \qquad (\omega \ll \gamma).$$

Again, the emissivity varies as $1/\lambda^2$ in the far infrared. But various observations of emission from interstellar dust suggest that the wavelength dependence of emissivity is closer to $1/\lambda$ than to $1/\lambda^2$ (Seki and Yamamoto, 1980). This may be a consequence of the failure of the conditions underlying the $1/\lambda^2$ dependence—the particles are *crystalline* and *spherical*—to be satisfied.

For the insulating solid it was assumed that far infrared frequencies were well below any absorption band. But the allowed optical transitions in an amorphous, insulating solid are not necessarily confined to bands; that is, there may be continuum absorption extending into the low-frequency region. The characteristics of amorphous grains as far-infrared emitters have been discussed by Seki and Yamamoto (1980), who also pointed out the $1/\lambda^2$ dependence discussed in the preceding paragraph. Measurements of far-infrared absorption by small particles of amorphous silicates (Day, 1979) and amorphous graphite (Koike et al., 1980) have in fact shown that the absorption efficiency varies approximately as $1/\lambda$.

Particle shape can strongly affect the far-infrared emission spectrum of metallic particles, for which the region of negative ϵ' is large; graphite also falls into this category. This is evident from measured absorption by small aluminum particles (Fig. 12.20), which we have interpreted using a distribution of ellipsoidal shapes. Note that the wavelength dependence of absorption by spheres is vastly different from that by a collection of particles distributed in shape.

From these considerations we conclude that the failure of the emission spectrum of interstellar dust to vary as $1/\lambda^2$ in the far infrared, which is predicted for small crystalline spheres, may be the result of either noncrystallinity or nonsphericity (or both). Therefore, the infrared emission spectrum may not prove to be as uniquely diagnostic of interstellar grain characteristics as it once was thought to be.

14.5.9 Summary of Observations and Their Interpretations

We summarize in Table 14.2 the observed characteristics of interstellar dust together with their most common interpretations. What is meant by a "common interpretation" is to some extent a matter of opinion, and this table naturally reflects ours. Other interpretations have been published in the many papers on interstellar dust; these can be found in the review articles cited at the beginning of this section.

Table 14.2 Summary of Interstellar Dust Observations

Observation	Interpretation
Reddening of visible light	Particles smaller than λ
Prominent extinction peak at 2170 Å (5.7 eV)	Surface plasmon in graphite
Continued rise in extinction to at least 12 eV	Extinction by the small size component
Extinction knee near 3 eV	Scattering by the large size component
Many narrow bands (diffuse bands) in the visible	Unidentified
Absorption and emission bands at 9.7 and 18 μm	Vibrational modes in disordered silicate grains
Emission band near 11 μm associated with carbon stars	Shape broadened vibrational modes in SiC
Linear polarization peaking in the visible	Asymmetric particles aligned in galactic magnetic fields
Circular polarization	Changing grain alignment; aligned grains acting like retarder
Absorption band at 3.07 μm	H_2O and NH_3 ice coatings on particles in protected regions
Far infrared emission decreasing as $\sim 1/\lambda$	Amorphous silicates or carbon; possible shape effects

14.6 PRESSURE DEPENDENCE OF INTRINSIC OPTICAL SPECTRA USING SMALL PARTICLES

Lattice parameters of crystalline solids can be varied over appreciable ranges by subjecting them to very high pressures. The development of diamond-anvil pressure cells (see, e.g., Block and Piermarini, 1976) and a simple technique for monitoring pressure using the fluorescence spectrum of a tiny chip of ruby inside a cell (Forman et al., 1972) has made it possible to study the effects of pressures up to more than 400 kbar on the optical properties of solids (and liquids). But the class of optical effects involving electronic excitations has been difficult to study in pressure cells. Absorption is so strong that very thin films must be used for transmission studies; but the structure of such films is often different from that of bulk crystalline solids because of the way films are grown on substrates. And specular reflection techniques are impractical for samples under pressure because of small apertures, many reflecting surfaces, and relatively long optical paths in pressure cells. It is possible, however, to exploit the advantages of small particles—it is easier to make small crystals than large crystals—as samples and study optical effects by measuring the dependence of spectral transmission on pressure.

An example of a spectral feature of possible interest is the exciton peak in MgO near 7.6 eV (see Figs. 9.5 and 10.1). This peak has been studied primarily by reflection from cleaved crystals of MgO. But careful inspection of Fig. 11.2 reveals that the exciton peak is also expected to appear clearly in extinction by MgO particles provided that they are sufficiently small.

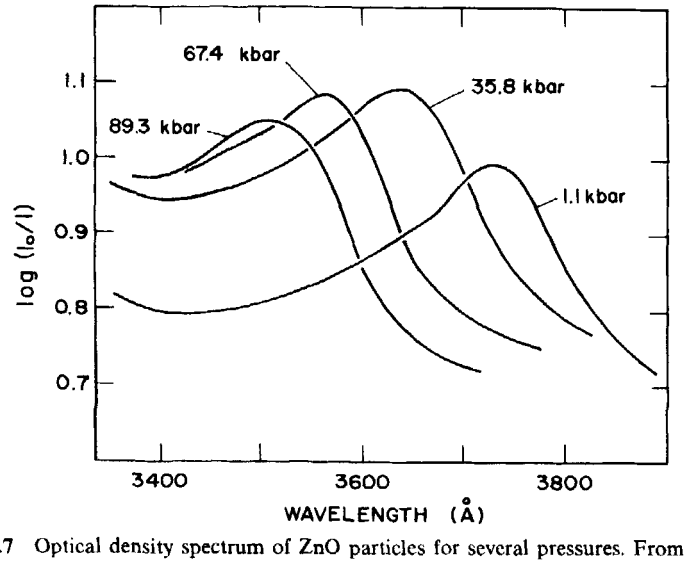

Figure 14.7 Optical density spectrum of ZnO particles for several pressures. From Huffman et al. (1982).

This idea of using small particles to obtain information about solids under pressure has been explored by Huffman et al. (1982), who studied the band gap exciton in ZnO at pressures up to 107 kbar. A smoke consisting of small crystalline particles (~ 0.1 μm) of ZnO was formed by arc-vaporizing metallic zinc in air and collecting the particles on the inner surface of one of the diamonds that form both the windows and the anvils of the pressure cell. Spectral transmission measurements taken by simply placing the sample-laden cell in a double-beam spectrophotometer clearly revealed the intrinsic band gap exciton (near 3730 Å at ambient pressure), the characteristics of which were then followed as pressure was increased to 107 kbar. A progressive shift of the band to about 3490 Å was observed (Fig. 14.7), and the exciton energy (position of the absorption edge) increased linearly with pressure. The primary aim of this experiment was not, however, to study the ZnO exciton but rather to demonstrate a new technique for studying optical effects in solids under pressure by using small particles.

14.7 GIAEVER IMMUNOLOGICAL SLIDE

A simple visual technique for investigating immunological reactions has been devised by Giaever (1973). A discontinuous film composed of small metallic particles, or islands, is evaporated onto a glass slide, and a monolayer of antigen adsorbed onto this surface; indium was first used, later an indium–gold alloy (Giaever and Laffin, 1974). The occurrence of an antigen–antibody reaction is indicated by darkening of the slide. The mechanism for the observed darkening was not discussed in detail; it was merely mentioned in passing that it was the result of increased scattering. But small metallic particles absorb light more strongly than they scatter it, and it seems clear that what is observed may be attributed to a shift of the surface mode frequency because of the coating on the metallic particles. The Giaever immunological slide is therefore a biomedical application of surface modes in small metallic particles, which were discussed at length in Chapter 12.

Treu (1976) measured transmission spectra (optical density) for indium films of the type used for immunological slides. His calculations based on Mie theory led him to the conclusion that this theory was not compatible with observations. In particular, calculations for spheres of diameter 1390 Å showed a feature that was not observed in experiments. Although calculations for spheres half this size did not show this feature, the wavelength of maximum optical density was much shorter than that observed.

It is not surprising, however, that Mie theory is inadequate in this instance: the indium particles are not spheres, they are more nearly oblate spheroids with (average) major and minor diameters of about 1390 and 368 Å.

Although the indium particles are not small compared with the wavelength in all directions, they are sufficiently small (368 Å) along the direction of propagation of the incident light that Rayleigh theory is a good approximation. The unobserved feature calculated for 1390-Å spheres is therefore easy to

explain: such spheres are, at visible and ultraviolet frequencies, sufficiently large that higher-order modes are excited; this was shown in Fig. 12.1 by a set of calculations for progressively larger SiC particles. The disparity between the measured frequency of peak extinction and that calculated for 700-Å spheres is also readily explicable: this frequency is strongly dependent on shape and can extend all the way from the plasma frequency ω_p (typically in the ultraviolet) down to radio frequencies.

Interpretation of the observed transmission spectra of immunological slides is complicated by the close separation of the indium particles; Treu (1976), for example, reports areal coverages of 68%. Also, the particles, even if they are uncoated, are not embedded in a single homogeneous medium: there is air on one side of them and glass on the other. And while the particles are most definitely not spheres, they are not identical oblate spheroids: there is a distribution of shapes. But we have taken the view throughout this book that understanding small-particle effects begins with isolated, uncoated spheres. Each of these restrictions can then be successively removed to assess their relative importance in determining spectral features.

Indium is nearly a free-electron metal with a plasma frequency of about 11.5 eV, which corresponds to a wavelength λ_p of 1080 Å (Koyama et al., 1973). It follows from (12.28) that the wavelength λ_s of maximum absorption by a small metallic oblate spheroid illuminated by light incident along its symmetry axis is approximately

$$\lambda_s = \lambda_p \sqrt{\frac{\epsilon_m - L_1(\epsilon_m - 1)}{L_1}}, \tag{14.6}$$

where ϵ_m is the dielectric function of the surrounding medium; the geometrical factor L_1 takes on all values between 0 (disk) and $\frac{1}{3}$ (sphere). The particles are on a glass slide, so let us take ϵ_m to be 1.625, the average of that of glass (2.25) and air. For a sphere, therefore, $\lambda_s = \lambda_F$ (the wavelength corresponding to the Fröhlich frequency) is about 2230 Å, which is close to the value 2500 Å calculated for a 700 Å sphere by Treu (1976).

As the sphere is flattened into a disk the position of maximum absorption shifts to longer wavelengths. For example, if $c/a = 368/1390$, it follows from Fig. 5.6 that L_1 is about 0.19 and from (14.6) that λ_s is 3040 Å. This is an appreciable shift—over 800 Å—but still short of the measured value 4100 Å. Our analysis, however, implicitly assumed isolated spheroids, a condition that was not satisfied in the experiments.

We can estimate the magnitude of the shift attributable to interaction between particles by appealing to the Maxwell Garnett theory (Section 8.5). This theory is strictly applicable only to a medium consisting of small particles distributed throughout a volume, whereas the slides consist of a single layer of particles on a surface. Nevertheless, for our limited purposes here the Maxwell Garnett theory is adequate.

It follows from (8.47) that the average dielectric function of a suspension of identical oblate spheroids is

$$\epsilon_{av} = \frac{(1-f)\epsilon_m + f\epsilon\lambda_1}{1-f+f\lambda_1}; \qquad \lambda_1 = \frac{\epsilon_m}{\epsilon_m + L_1(\epsilon - \epsilon_m)}, \tag{14.7}$$

where the electric field is parallel to the major axes. If (14.7) is expanded to terms *linear* in the particle volume fraction f, the wavelength where ϵ''_{av} is a maximum is given by (14.6), as expected. But if ϵ''_{av} is truncated after the *quadratic* term in f, the wavelength of maximum absorption $\lambda_s(f)$ is given by

$$\lambda_s(f) = \lambda_s\left[1 + \frac{1}{2}\frac{f\epsilon_m}{L_1 + \epsilon_m(1-L_1)}\right].$$

Thus, the effect of decreasing the separation between particles is to shift the position of maximum absorption to longer wavelengths, which is consistent with the experimental observations.

The absorption spectrum of isolated indium spheres differs from that of closely packed oblate spheroids in that the peak shifts from 2230 Å to 4100 Å; about half of this shift is attributable to particle shape and half to particle interaction. Indium particles on immunoiogical slides are not identical, however, but are distributed in size and shape about some mean; this tends to broaden the spectrum.

The observed darkening of the indium slides results from a shift of the absorption peak because of the coating on the particles. Because of the cumbersomeness of the expressions for coated ellipsoids (Section 5.4) this shift can be understood most easily by appealing to (12.15), the condition for surface mode excitation in a coated sphere. For a small metallic sphere with dielectric function given by the Drude formula (9.26) and coated with a nonabsorbing material with dielectric function ϵ_2, the wavelength of maximum absorption is approximately

$$\lambda_s = \lambda_F\left[1 + \delta(\epsilon_2 - \epsilon_m)\frac{\epsilon_2 + 2\epsilon_m}{\epsilon_2 + 2\epsilon_m\epsilon_2}\right],$$

where terms of higher order in δ, the coating thickness relative to the core radius, are neglected. If ϵ_2 is greater than ϵ_m, therefore, the effect of the coating is to shift the position of peak absorption to longer wavelengths, which is also in accord with observations. Moreover, to first order at least, this shift is proportional to the thickness of the coating and increases with increasing ϵ_2.

Our assertion that the darkening of immunological slides, which are observed by transmitted light, is primarily an absorption rather than a scattering phenomenon can be supported by a simple calculation. The cross sections for absorption and scattering by a single, uncoated oblate spheroid illuminated

along its symmetry axis are (see Section 5.5)

$$C_{\text{abs}} = \mathrm{k}\,\mathrm{Im}\{\alpha_1\}; \qquad C_{\text{sca}} = \frac{\mathrm{k}^4}{6\pi}|\alpha_1|^2$$

$$\alpha_1 = 4\pi a^2 c \frac{\epsilon - \epsilon_m}{3\epsilon_m + 3L_1(\epsilon - \epsilon_m)}.$$

If we use the values of ϵ' and ϵ'' measured by Koyama et al. (1973), the ratio of maximum absorption to maximum scattering is approximately

$$\frac{C_{\text{abs}}}{C_{\text{sca}}} \simeq 6 \qquad (\lambda \simeq 3000\ \text{Å})$$

for $L_1 = 0.19$, $a = 695$ Å, and $c = 184$ Å. Absorption therefore dominates extinction in this instance.

Biology is an unlikely field in which to find an application of surface modes in small metallic particles. After all, the optical properties of particles of biological origin are very much unlike those of metals. Yet the Giaever immunological slide is just such an application. Moreover, it exemplifies many of the salient characteristics of surface modes which were discussed in Chapter 12: their strong dependence on particle shape, coating, and the surrounding medium.

14.8 MICROWAVE ABSORPTION BY MACROMOLECULES

A rather grisly example of biological effects of microwave radiation is provided by the story, possibly apocryphal, of the woman who put her cat in a microwave oven to dry after it had come in out of the rain. The cat exploded! And one hears tales of crows and seagulls being shot out of the sky with intense microwave beams.

Regardless of the truth of these stories, it is undeniable that microwave radiation can be hazardous to life. One damage mechanism is merely intense heating of the water bound up in all living organisms. It is clear, therefore, that the potential hazard of radiation of a given frequency depends on the optical constants, particularly ϵ'', of water at that frequency. For example, at room temperature the maximum value of ϵ'' occurs at about 20 GHz (see Fig. 9.15), that is, at the relaxation frequency $1/2\pi\tau$, where τ is the relaxation time in (9.41).

Although liquid water is usually looked upon as a single, unvarying substance, its structure near surfaces may be quite different from that of "free" water. Interaction between water molecules and an immediately adjacent surface orients these molecules, and this orientation can extend for several molecular diameters into the bulk liquid. A very clear and succinct description of this mechanism was given by Henniker (1949): "Although the powerful

forces involved are very short range, they are transmitted by successive polarization of neighboring molecules to an impressive depth. The analogy is with a magnet of very limited range of appreciable direct interaction which nevertheless can lift or hold a piece of iron at a considerable distance if there is an intermediate chain of iron fillings or pieces of iron in between." Many papers have been written about the properties of liquids at interfaces, the earliest of which were reviewed by Henniker (1949); more recently, Drost-Hansen (1969) thoroughly examined the evidence for the existence of ordered water near solid interfaces.

If the structure of water depends on distance from a surface, so must its physical properties, including its dielectric function. We noted in Section 9.5 that at microwave frequencies the dielectric function of water changes markedly when the molecules are immobilized upon freezing; as a consequence, the relaxation frequency of ice is much less than that of liquid water. Water irrotationally bound to surfaces is therefore expected to have a relaxation frequency between that of water and ice.

Water molecules are oriented at the surfaces of macromolecules as well as at solid surfaces. For example, Bernal (1965) refers to a "regular formation of ice" surrounding most protein molecules, although by "ice" he does not mean free water ice. Bound water in hydration shells surrounding macromolecules in aqueous solutions is sometimes denoted as lattice-ordered or ice-like and has been taken into account in interpreting the dielectric functions of such solutions (Buchanan et al., 1952; Jacobson, 1955; Pennock and Schwan, 1969).

The possible consequences of irrotationally bound water for microwave absorption by biological materials are twofold. Calculations of the rate of energy deposition using the dielectric function of free water may be appreciably in error at frequencies well below its relaxation frequency, which is greater than that of bound water. Moreover, the bound water is confined to thin hydration shells around macromolecules, so the enhanced energy absorption in these shells may cause localized disorganization. Dawkins et al. (1979) put forward these ideas and supported them with calculations of power deposition for a simple model of a hydrated molecule: a sphere of radius 5 nm surrounded by a shell of water two molecules thick; these calculations were based on the theory of Section 8.1—only the first term in the series is needed because of the extremely small size parameter—and the dielectric function (9.41) with various relaxation frequencies. Although the validity of using macroscopic theory for a single macromolecule coated by only two layers of water molecules is uncertain, their results are likely to be qualitatively correct and, consequently, are worth contemplating.

The volumetric power deposition calculated for bound water was appreciably greater—up to about five times—than that for free water; the maximum difference occurs near the bound water relaxation frequency. This enhanced energy deposition is localized in the bound water shell and therefore may cause more damage than if it were distributed uniformly throughout the medium. But Dawkins et al. consider the enhancement of biological damage by localiza-

tion still to be speculative because of uncertainties about the rate of energy transfer from the shell to its macromolecule host and to its surroundings. Nevertheless, ignoring the differences between the dielectric functions of bound and free water may have important consequences. Dawkins et al. illustrate this with a particular microwave injury the mechanism for which is well understood. Cataracts are induced by microwave radiation because it is absorbed by lens water and the resulting temperature increase denatures lens proteins. About 65% of the weight of the lens is water, at least 40% of which is bound water. If all the water were taken as free, as is usual in estimating microwave energy absorption in biological materials, the rate of heating by microwave radiation in the frequency range 0.3–3 GHz could be underestimated.